NASA CR-165521

INERT GAS ION THRUSTER

(NASA-CR-165521) INERT GAS ION THRUSTER
Final Report, Mar. 1978 - Dec. 1980 (Xerox
Electro-Optical Systems, Pasadena) 90 p
HC A05/MF A01 CSCL 21C
N82-212
Unclas
G3/20 09467

PREPARED FOR

NATIONAL AERONAUTICS AND SPACE ADMINISTRATION

LEWIS RESEARCH CENTER

CONTRACT NO. NAS3-21345

Final Report

December 1980

NASA CR-165521

INERT GAS ION THRUSTER

PREPARED FOR
NATIONAL AERONAUTICS AND SPACE ADMINISTRATION
LEWIS RESEARCH CENTER

CONTRACT NO. NAS3-21345

Final Report

December 1980

1. Report No.
CR-165521

2. Government Accession No.

3. Recipient's Catalog No.

4. Title and Subtitle
Inert Gas Ion Thruster Program

5. Report Date
December 1980

6. Performing Organization Code

7. Author(s)
William D. Ramsey

8. Performing Organization Report No.
2372-5009

9. Performing Organization Name and Address
Xerox Electro-Optical Systems
300 N.Halstead
Pasadena, California 91107

10. Work Unit No.

11. Contract or Grant No.
NAS 3-21345

12. Sponsoring Agency Name and Address
National Aeronautics and Space Administration
Lewis Research Center
21000 Brookpark Road
Cleveland, Ohio 44135

13. Type of Report and Period Covered
Final Report
March 1978-December 1980

14. Sponsoring Agency Code

15. Supplementary Notes
Project Manager: Shigeo Nakanishi, NASA-Lewis Research Center, Cleveland, Ohio

16. Abstract

Inert gas performance tests were conducted with three types of 12 cm diameter magneto-electrostatic containment (MESC) ion thrusters. The types tested included: a hemispherical shaped discharge chamber with platinum-cobalt magnets; three different lengths of the hemispherical chambers with samarium-cobalt magnets; and three lengths of the conical shaped chambers with aluminum-nickel-cobalt magnets.

The best argon performance was produced by a 8.0 cm long conical chamber with alnico magnets. This thruster assembly achieved 54 to 80 percent argon mass utilization efficiency at 240 to 310 eV/ion of single charged ion equivalent beam.

The best xenon high mass utilization performance was obtained with the same 8.0 cm long conical thruster. The thruster produced xenon utilizations of 90 to 97 percent at 210 to 280 eV/ion of singly charged ion equivalent beam. At less than 87 percent utilization efficiency, the best xenon performance was produced with the 5.7 cm long hemispherical thruster fitted with samarium-cobalt magnets. The hemispherical thruster obtained 75 to 87 percent mass utilization at 185 to 205 eV/ion of singly charged ion equivalent beam.

17. Key Words (Suggested by Author(s))
Electric Propulsion
Argon & Xenon Ion Source
12 cm Ion Thruster

18. Distribution Statement
Unclassified - Unlimited

19. Security Classif. (of this report)
Unclassified

20. Security Classif. (of this page)
Unclassified

21. No. of Pages

22. Price*

* For sale by the National Technical Information Service, Springfield, Virginia 22161

NASA-C-168 (Rev. 10-75)

SUMMARY

Inert gas performance tests were conducted with three magneto-electrostatic containment (MESC) ion thrusters. The first of these was a 12 cm diameter hemispherical thruster with platinum-cobalt boundary magnets. The pt-co magnet thruster was originally designed for cesium operation under contract to COMSAT Corporation in 1974 and was loaned to XEOS for this program. The second was a 12 cm MESC hemispherical thruster equipped with samarium-cobalt magnets. The third thruster tested was a 12 cm conical MESC thruster designed and fabricated for maximum flexibility in discharge chamber geometry.

Various physical configurations of the thrusters were tested to determine which produced the best inert gas performance. The best high mass utilization performance was produced by the 8.0 cm length 1.8 cm magnet spacing conical thruster assembly. The thruster assembly achieved 50 to 80 percent argon mass utilization efficiency at 240 to 310 eV/ion. Xenon performance of the same thruster achieved 60 to 97 percent mass utilization at 240 to 380 eV/ion.

Best discharge chamber performance at somewhat lower mass utilization efficiency was obtained with the 5.7 cm long samarium-cobalt magnet hemi thruster. Argon utilization of 60 to 68 percent was achieved at 215 to 260 eV/ion. The same thruster produced 70 to 87 percent xenon utilization at 185 to 225 eV/ion.

Tests were conducted with different discharge chamber lengths and magnet spacings. Hemi thruster lengths of 5.7, 8.0 and 10.3 cm were performance tested. A 5.7 cm length conical thruster was tested with a 1.3 cm magnet spacing while a 8.0 cm thruster assembly under went testing with magnet spacings of 1.3 and 1.8 cm. A 9.0 cm long conical thruster with a 2.3 cm magnet spacing was also tested.

Addition of a decel electrode to a set of uncompensated grids reduced the minimum operable net accelerating potential but did not significantly affect the beam spreading characteristics. The percentage of double-charged ions in the beam was obtained from time-of-flight measurements. In the conical thruster, the percentage increased with discharge chamber length but decreased with wider magnet spacings.

CONTENTS

CONTENTS (contd)

CONTENTS (contd)

PRECEDING PAGE BLANK NOT FILMED

ILLUSTRATIONS

ILLUSTRATIONS (contd)

SECTION 1

INTRODUCTION

Work on this program was sponsored by NASA Lewis Research Center under contract NAS3-21345. The period covered by this final report extends from April 1979 through September 1980.

1.1 BACKGROUND - ION PROPULSION

A growing interest in ion propulsion has recently arisen from the recognized need to place large payloads into synchronous orbits or planetary-trajectories. Ion propulsion thrust systems are leading candidates for these applications. Until a few years ago most ion thruster development concentrated on mercury or cesium propellent usage. Mercury, has a 5.7×10^{-12} cm^2 cross section and a 10.4 eV first ionization potential. Ionization ease allowed efficient mercury performance to be achieved without being overly concerned with wall recombination losses or maximizing the ionizing electron diffusion path length to the anode. This was particularly true in the case of a large thruster with a large volume-to-surface-discharge chamber wall area ratio as exemplified by the 30 cm mercury thruster[1]. However, mercury has well known environmental drawbacks in space and terrestrial applications. Cesium also has negative environmental constraints.

Inert gas have very high vapor pressures and are not toxic or alkaline but are harder to ionize than either mercury or cesium. Xenon has an atomic mass of 132 and a first ionization potential of 12.1 eV. Argon has an atomic mass of 40 and first ionization potential of 15.7 eV with an ionization cross section half that of mercury or xenon. The scarcity and cost of xenon will probably restrict the usage of inert gases in large primary propulsion thruster systems to the more plentiful argon.

Early tests demonstrated that the large divergent field thruster has poor argon performance with low mass utilization and high eV/ion[2]. Improved discharge chamber technology was needed to make inert gas thrusters competitive with the developed mercury technology. Mercury[3] and cesium[4] tests with MESC thruster[5] achieved performance levels surpassing divergent field thrusters of similar size and showed particular promise in inert gas application. A similar design, multipole thruster, was tested with argon and xenon at Colorado State University by H. Kaufman[5] and showed substantial improvement over the divergent field thruster performance. Later MESC tests[6] under the sponsorship of LeRC showed further improvements in inert gas mass utilization and eV/ion performance.

1.2 MESC CONCEPT

The MESC discharge chamber concept was first described by R.D. Moore[7] in 1968. He predicted the MESC discharge chamber would improve ion thruster performance with any propellent by limiting ion loss from the discharge plasma to the walls and provide a method of controlling the electron diffusion current. Moore based these predictions on calculation from classic physics after Spitzer.[8] Moore subsequently conducted cesium tests with a 12 cm hexagonal cross section MESC thruster and obtained excellent performance.[7] Later the same discharge chamber modified for mercury[3] operation again produced outstanding performance. Ninety percent mercury mass utilization efficiency was produced at a discharge energy of 160 eV/ion. MESC thruster mercury performance reduced discharge energy consumption 35 percent compared to similar mass utilization operation of a 15 cm diameter divergent field mercury operation thruster.[9]

MESC discharge geometry is composed of alternate rows of magnets and anodes parallel to the grid system. Adjacent rows of magents have alternate polarity. This magnetic circuit produces a large boundary magnetic field at the anode surface that cancels out in the discharge plasma volume. The original cesium version had a plasma or auxiliary anode to sustain the discharge, although Moore had predicted boundary anodes could perform this function. Moore's predictions were confirmed in the mercury tests when the plasma anode was removed and the boundary anodes were located further in the discharge plasma. Removal of the plasma anode permitted better control of the electron diffusion current and reduced discharge energy consumption 20 percent.

Inert gas tests[6] with the same 12 cm hexagonal MESC thruster found the electron diffusion current to the anodes was not proportional to $1/B^2$ as predicted from classical physics. Further inert gas tests without the hemispherical shaped MESC thruster confirmed the anode diffusion current was proportional to $1/B$ instead. The $1/B$ relationship implied the electrons were reaching the anodes by Bohm diffusion rather than by classical diffusion.

1.3 MESC OPERATING PRINCIPLES

Bohm[10] found the electron diffusion across a magnetic field was directly proportional to the Maxwellian electron distribution temperature and inversely proportional to the magnetic flux density. Electron diffusion defined by this relationship was semi-empirically derived from a fully ionized argon plasma operating under conditons similar to those found in an ion thruster. Chen[11] reports other workers confirmed Bohm's diffusion coefficient and found that electron diffusion in regimes corresponding to ion thruster operation are also proportional to the plasma density gradient. The neoclassic Bohm diffusion referenced by Chen is:

$$D = \frac{1}{16} \frac{kT_e}{qB_A} \nabla n \tag{1}$$

where:

k = Boltzmann constant

T_e = Maxwellian distribution electron temperature

B_A = Component of the magnetic field parallel to the discharge chamber walls

q = Electron charge

n = Plasma density gradient

The Maxwellian electron temperature, T_e, is the minimum energy an electron needs to diffuse to the anode. In a typical thruster discharge plasma, these lower energy electrons are present in order of magnitude greater concentrations than the high energy or primary electron and, therefore, have almost all the collisions in either classic or neoclassic Bohm diffusion.

Kaufman[12] found Bohm diffusion should be further modified for multipole thruster application. Assuming zero electric field close to the anode and uniform density in the diffusion region, Kaufman showed the wall/anode diffusion current density is given by:

$$j \propto \frac{kT_e \, n_e}{13 \int B dx} \qquad (2)$$

where n_e is the electron density and $\int B dx$ is the integrated flux density from magnet pole surface (MPS) to the field zero midway between adjacent magnets. The magnets pole surface is shown schematically in figure 1-1.

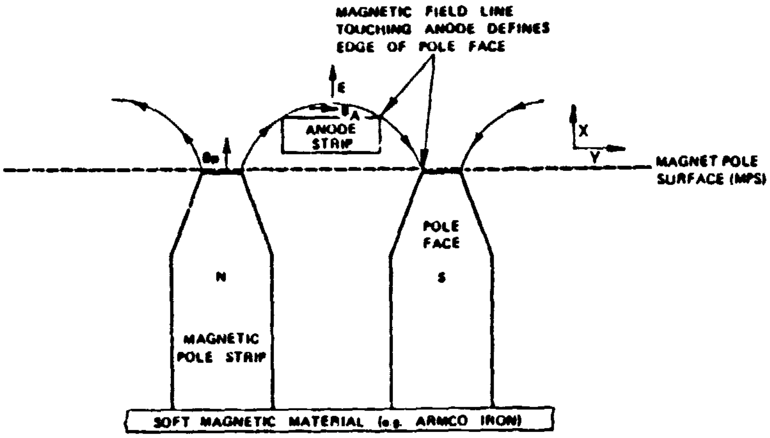

Figure 1-1. Schematic of Magnet Pole Surface

Robinson[13] showed the multipole magnetic field midway between magnets of opposite polarity is:

$$B = B_p \exp -1.5\,(x/d + 0.5)^2 \qquad (3)$$

where:

B_p = magnetic field at the magnet surface
x = displacement between the MPS and anode surface
d = center-to-center spacing of adjacent magnets

Typically, anodes in a MESC design thruster are located far from the MPS where $x > d$. Hence, B is a slowly varying function of x and $\int Bdx$ can be approximated with:

$$\int Bdx \propto B_A x$$

where B_A is the field at the surface of the anode parallel to the chamber walls. Given the Maxwellian electron temperature and electron density in the discharge plasma, it is possible to adjust anode magnetic field for the optimum current density to a first approximation with the relationship:

$$j \propto \frac{kT_e}{B_A} n_e$$

The magnetic field-anode geometry also limits ionic recombination losses in the MESC discharge chamber. Using cusped field ion sources, other workers[14] found the ionic recombination losses were inversely proportional to the magnetic field. Two investigators[15,16] independently determined ionic recombination losses were proportional to the square root of the product of primary electron and ionic Larmor radii or the "hybrid radius" defined by the following equation in MKS units:

$$P_x = \text{Larmor Radius} = \frac{m_x v}{q\,Bp} \qquad (4)$$

$$\text{Hybrid Radius} = (P_i P_e)^{1/2} \qquad (5)$$

where:

m_x = electron or ionic mass
v = component of the ion or electron velocity orthogonal to the magnetic field
q = electronic charge
B_p = magnetic field at the pole

In the hybrid radius definition, p_e and p_i are the electron and ion Larmor radii, respectively.

The hybrid radius was found to be the width of the ion loss area adjacent to the magnet pole face along the discharge chamber walls. The total ion loss region was the product of the magnet length and the twice the hybrid radius. This relationship was found to apply to several gases under a wide range of operating conditions that included argon plasma at temperatures and densities similar to those found during nominal ion thruster operations.

In the MESC discharge chamber, the magnet surface area exposed to the plasma are defined by the magnetic field lines connecting the magnet surface and the anode edges or critical field lines. The charged particles reaching these lines are collected at the anodes while those that do not are reflected or lost at the magnet surfaces defined by the critical magnetic field lines and hybrid radius illustrated in figure 1-1. Increases in the magnet pole field strength cause the anodes to be located further from the MPS to keep a constant magnetic flux density over the anode surfaces and maintain the same plasma operating conditions. Thus, stronger magnets tend to reduce ion recombination losses by reducing both the magnet pole area defined by the anode geometry and the hybrid radius.

1.4 INERT GAS MESC THRUSTER DEVELOPMENT PROGRAM

NASA Lewis Research Center has supported a program for the development of MESC thruster inert gas operation. The program has encompassed three phases as described below.

1.4.1 INITIAL MESC THRUSTER INERT GAS DEVELOPMENT PROGRAM

The initial phase of the program converted the original 12 cm hexagonal MESC thruster from mercury to argon-xenon operation and optimized discharge chamber performance. The effort took place under contract NAS3-20393 and the detailed results were reported in CR-159423.

The 12 cm hex thruster argon and xenon performance curves from this phase are shown in figure 1-2. The performance plotted was corrected for ingestion of neutral backflow and double ion production. Discharge power consumption used to calculate the eV/ion was the sum of the total output from the keeper and anode power supplies. Hence, this calculation included the cathode electron emission plus the electron current produced by propellent ionization.

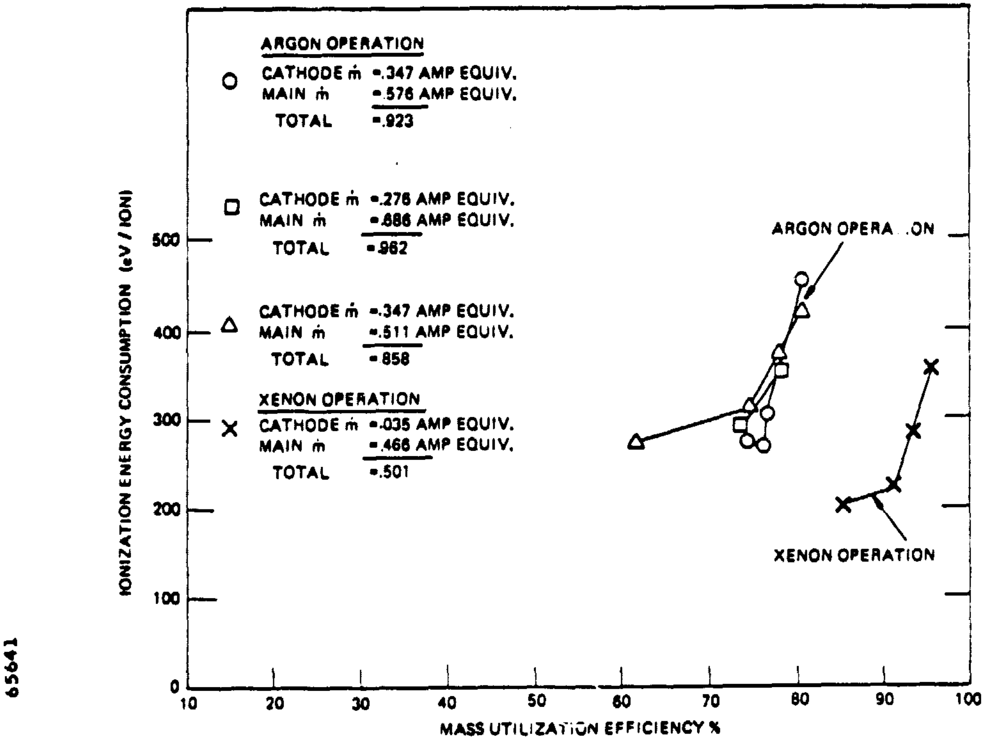

Figure 1-2. MESC Hexagonal Thruster Inert Gas Performance

1.4.2 FIRST INTERIM REPORT

This work was performed under NASA contract NAS3-21345 entitled "Inert Gas Ion Thruster Development," administered by NASA Lewis Research Center, Cleveland, Ohio and has been described in CR-159805. Tests were conducted with two existing MESC ion thrusters: a 12 cm hexagonal (hex) and a 12 cm hemispherical (hemi). The former was designed and built by XEOS in 1968; the latter was developed for COMSAT in 1974 and loaned to XEOS for use in this program. The purpose of the tests was to evaluate and optimize MESC thruster performance using argon and xenon propellents. Three categories of operational tests were conducted with the 12 cm hex MESC ion thruster. First, the tests confirmed the excellent inert gas performance previously reported with the hex thruster. Second, the tests defined the optimum discharge chamber plasma operating parameters; and third, the tests investigated the interactions between the operating parameters and hollow cathode subassembly. Results of the plasma/cathode investigation were used to select a cathode subassembly design for inert gas tests of the 12 cm hemispherical MESC thruster.

Hex MESC thruster tests achieved 79 percent argon mass utilization efficiency at discharge energy of 303 eV/ion and 90 percent xenon mass efficiency at 225 eV/ion. Optimum discharge chamber performance was achieved during mixed gas operation with argon hollow cathode flow and xenon main propellent. The xenon main flow configurations produced 92 percent ionic mass utilizaiton at 220 eV/ion.

The 12 cm hemispherical MESC thruster tests showed an unexpected loss in performance compared to that of the hex thruster. Preliminary performance mapping tests produced 67 percent argon mass utilization efficiency at 420 eV/ion and 90 percent xenon mass utilization at 389 eV/ion. The relatively poor hemi thruster inert gas performance was attributed to a shorter discharge chamber and a weaker, nonuniform peripheral magnetic field. This hypothesis was subsequently confirmed in a complementary IR&D program which showed hemispherical thruster performance could be improved by situating the boundary anodes in an uniform peripheral field.

1.4.3 FINAL REPORT

This is the final report of NASA contract NAS3-21345 and covers the program activity from April 1979 through September 1980. The inert gas ion thruster development effort in this phase had three primary goals. First, continue performance mapping tests with the 12 cm hemispherical-shaped MESC thruster using a three grid extraction system. Second, investigate the performance impact of stronger discharge chamber boundary magnets and lengthening discharge chamber. Third, design and test a new 12 cm MESC lab thruster designed expressly for inert gas operation.

The new thruster design incorporated a larger hollow cathode assembly, sized for inert gas operation and included the flexibility of testing MESC boundary-and-magnet geometry changes that could improve performance. These changes included three magnet center-to-center patterns and three discharge chamber lengths as well as several anode geometries.

1.5 REPORT ORGANIZATION

This report is divided into five sections. Section 2 describes the apparatus used in testing, and Section 3 presents the test results with the apparatus. Sections 4 and 5 discuss the conclusions and summarize the test results.

SECTION 2

APPARATUS AND PROCEDURE

2.1 12 CM HEMISPHERICAL MESC THRUSTER

The 12 cm hemispherical MESC thruster (hemi-MESC), was originally designed and built by XEOS for COMSAT as a flight prototype cesium ion thruster during a previous program[4]. The hemi-MESC design consisted of platinum-cobalt magnet rings of opposite polarity interspersed with stainless steel anode rings. Each pt-co ring was split so they could slip into the grooves in the chamber wall and the gap between the ends filled with a beryllium-copper plug to hold them in place. The rings were designed to be magnetized along hemispherical radii, that is, normal to the discharge wall with a 0.15 Tesla residual field at saturation.

Spaceflight requirements of minimum weight and structural integrity minimized flexibility and increased the difficulty of post-fabrication discharge chamber modification. Conversion from cesium to inert gas operation demanded several major changes in the discharge chamber design. A typical cesium discharge operated between 16 to 24 volts with a hollow cathode which was ignited and maintained without a keeper electrode or baffle structure. In order to convert the hemi-MESC to inert gas operation it was necessary to compensate for the higher plasma potential associated with efficient inert gas operation and modify the cathode magnet to accept a baffle and keeper electrode. From the Bohm relationship, higher plasma potential, (greater electron temperature), can be compensated by increasing the anode magnetic field. This was accomplished physically by moving the anodes closer to the magnet pole surface (MPS) shown in figure 1-1. A schematic of the hemi-MESC inert gas test assembly is shown in figure 2-1. A larger cathode magnet was used to allow for the additional cathode assembly hardware.

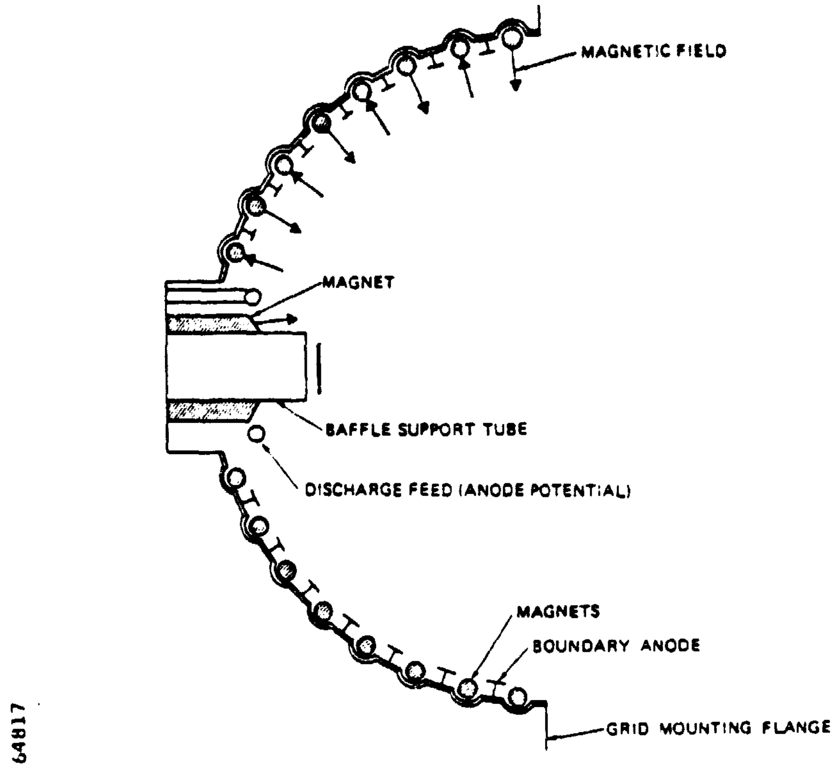

Figure 2-1. Cutaway Schematic of Hemi Thruster Test Assembly

2.1.1 HEMI THRUSTER PLATINUM-COBALT MAGNET ASSEMBLY

Large differences in the anode magnetic field were noted when the anodes were being relocated closer to the magnets for inert gas operation. Variation in the magnetic field made it necessary to modify anode ring design to achieve the most efficient inert gas operation.

Relocating the hemi thruster anodes at the calculated inert gas position produced an anode magnetic field that varied by a factor of two between points along a single anode. Several sections of the pt-co rings were found to be magnetized at angles up to 30 degrees from the wall normal which produced large variations in the anode field.

Anode magnetic field variations were partly the results of fabrication techniques. The magnets were fabricated up to 6.5 mm shorter than the groove length. Nonmagnetic beryllium-copper plugs were used to fill the end gaps to snug fit the magnets into the grooves of the discharge chamber wall. When the anodes were located relatively far from the magnets, in the position for cesium operation, these deviations from nominal were averaged out to produce a 15 percent point-to-point variation in anode magnetic field. However, as the anodes were brought closer to the magnets for the inert-gas operation, the impact of these variations increased causing wide deviations in anode magnetic field.

Several actions were taken to minimize the effects of the magnetic field variations on thruster operation. First, the beryllium-copper plugs in the larger diameter magnet rings were replaced with sections of platinum-cobalt rings with matching polarity. Second, the original one piece anode rings were divided into quarters to permit more flexibility in anode radial placement.

2.1.2 HEMI THRUSTER SAMARIUM-COBALT MAGNET ASSEMBLY

The platinum-cobalt magnets in the 12 cm hemi thruster were replaced with samarium-cobalt magnets to increase the boundary magnetic field and to provide a more uniform field. Short bar sections of samarium-cobalt were used instead of complete rings. The difficulty of fabricating and magnetizing ring shaped sections of samarium-cobalt led to the decision to use bar magnets sections 1.3 and 2.5 cm long. The magnet grooves in the chamber wall were fitted with half-round rings of magnetic iron to minimize the air gap in the magnetic circuit, as shown in figure 2-2. The largest air gap between the sm-co magnets and magnetic iron wall was held to 0.05 cm or less.

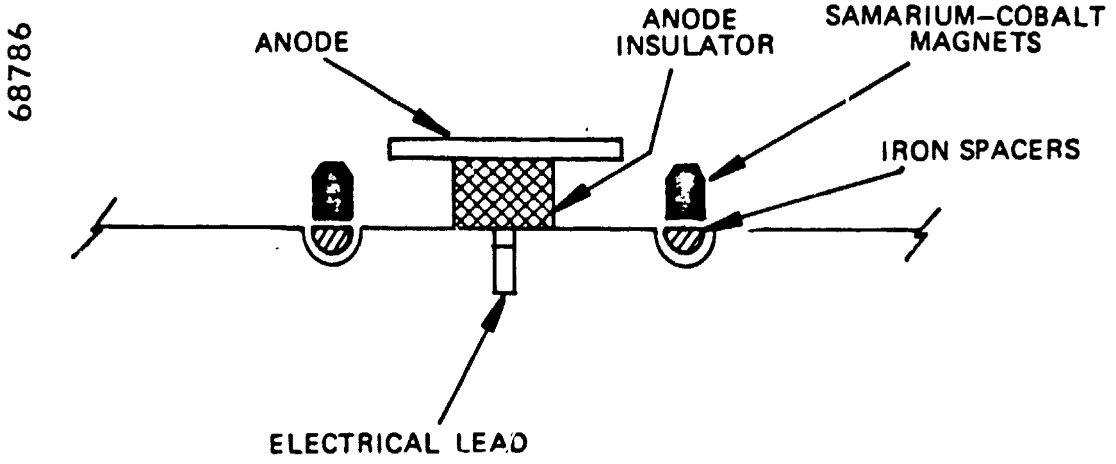

Figure 2-2. Schematic of Hemispherical Thruster Samarium-Cobalt Magnet Assembly

The samarium-cobalt magnets had a maximum residual field of 0.23 Tesla ±10 percent. The 0.4 cm wide, quartered anodes were mounted on adjustable length insulators providing rapid adjustment.

Active discharge chamber cooling was accomplished by a set of 3.2 mm diameter copper tubes attached directly to the magnet grooves of the discharge chamber. The coils were plumbed in parallel with sections of 6.4 mm diameter teflon tubing. A 50 cm length of teflon tubing was used to electrically isolate the discharge chamber-cooling coils assembly from ground. Similar flow rates were maintained through the individual coils by placing thin orifice plates in the shorter lengths.

The copper coils were held against the magnet grooves of the discharge chamber with strips of spotwelded stainless steel ribbon. Chamber wall temperature was monitored at three points to ensure thermal uniformity and to minimize the danger of magnet overtemperature. Ambient temperature nitrogen gas was used as a coolent to maintain wall temperture less than 200°C under most operating conditions. Thruster operation at maximum discharge power was limited to intervals of 10 minutes or less to prevent thermal degaussing of samarium-cobalt magnets.

2.1.3 HEMI THRUSTER DISCHARGE CHAMBER LENGTH TESTS

The samarium-cobalt discharge chamber assembly was lengthened in 2.3 cm increments. Cylindrical extension spool sections equipped with rings of samarium-cobalt magnets and anodes were fabricated and fitted with coils as shown in figure 2-3. The spools had a grid mounting flange on both ends which allowed attachment to the matching grid flange of the discharge chamber or subsequent spools. Discharge chamber lengths of 5.7, 8.0, and 10.3 cm were obtained by using one or more extension spools.

Figure 2-4 shows a photograph of the hemi-MESC thruster assembly with an attached extension spool and a nominal discharge chamber length of 8.0 cm. The "notches" in the surface toward the viewer are grid system attachment points.

ORIGINAL PAGE
BLACK AND WHITE PHOTOGRAPH

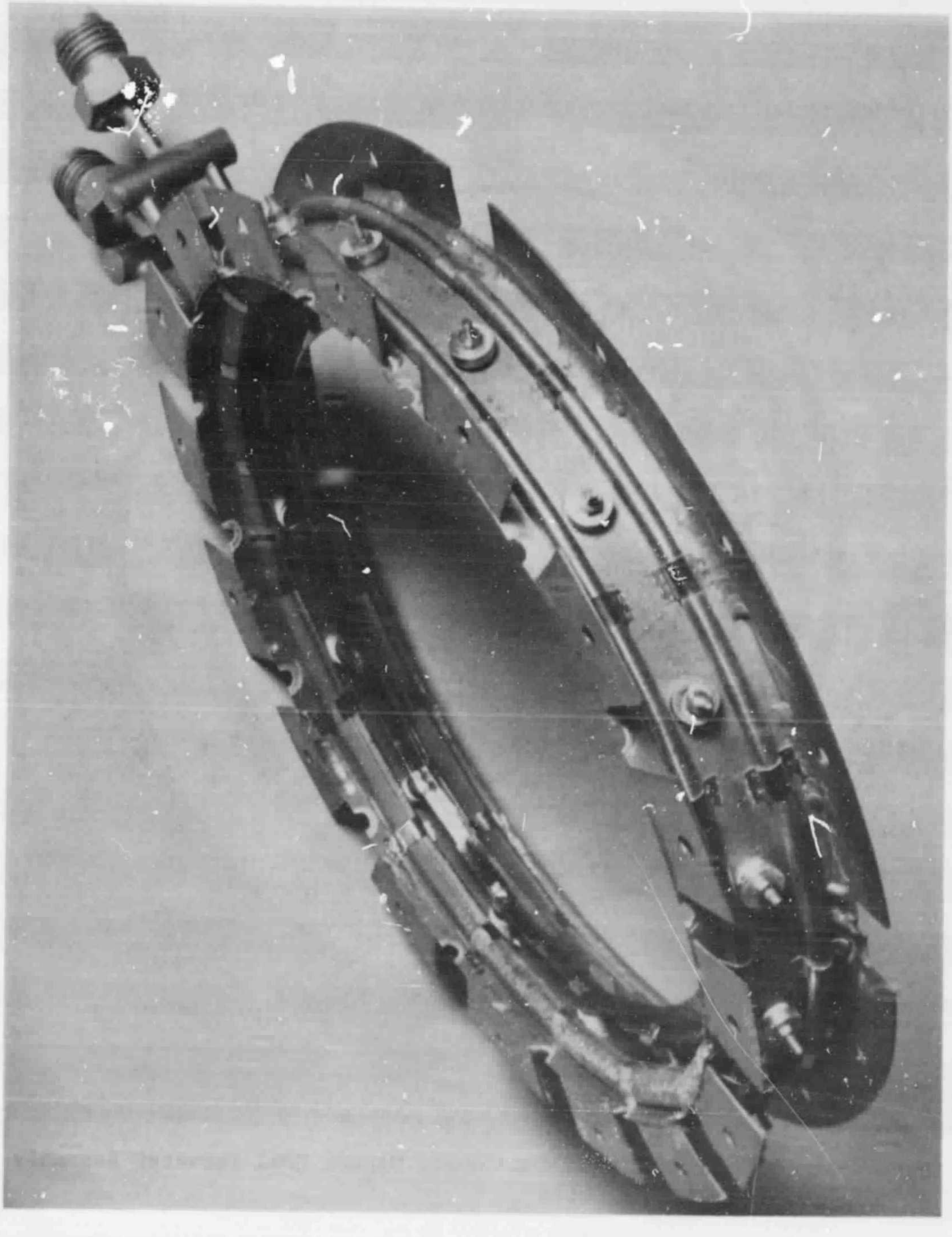

38058

Figure 2-3. Hemi Thruster Extension Spool with Samarium-Cobalt Magnets and Cooling Coils

ORIGINAL PAGE
BLACK AND WHITE PHOTOGRAPH

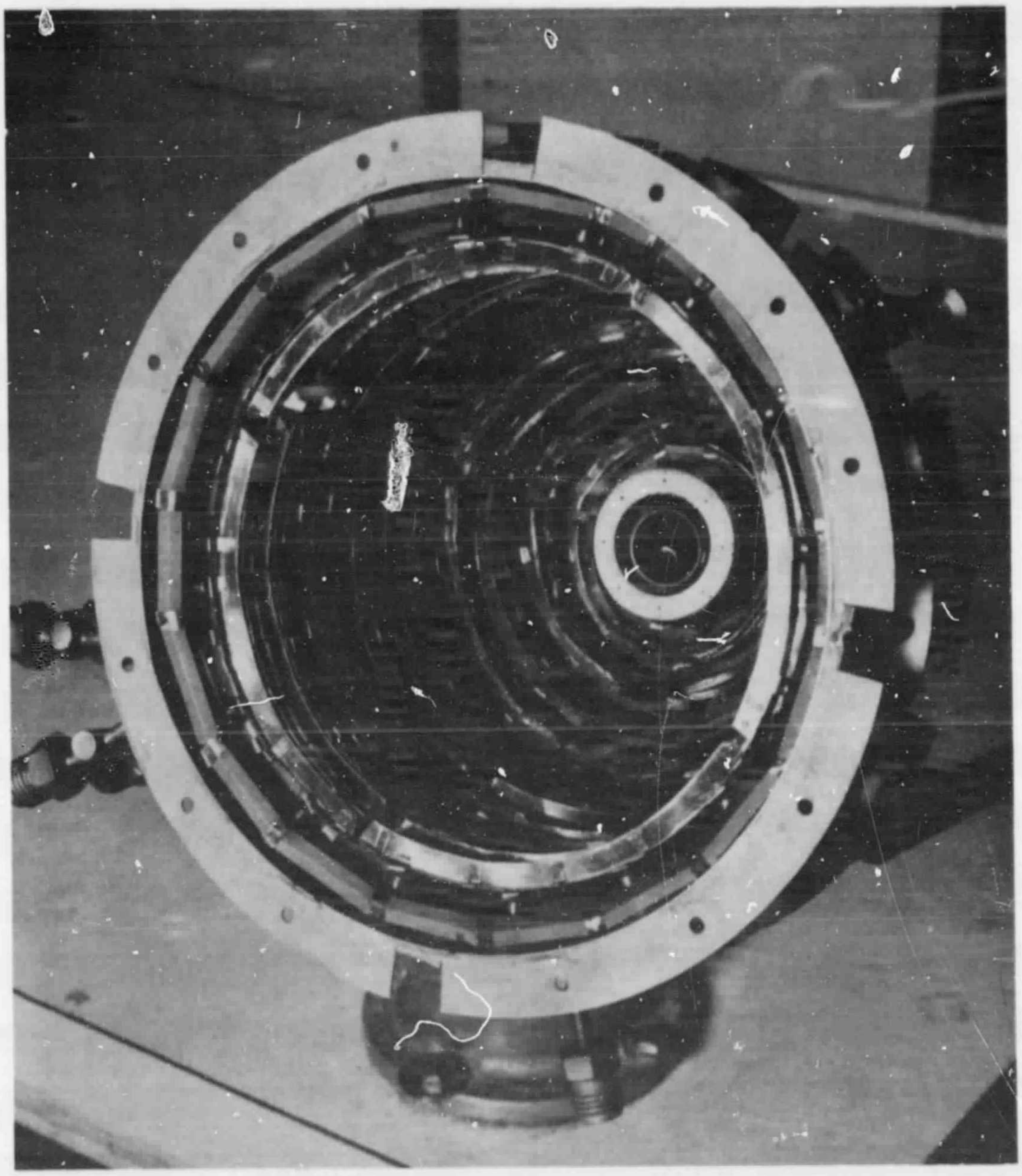

38051

Figure 2-4. 8.0 cm Long Samarium-Cobalt Magnet Hemi Thruster Assembly with Cooling Coils

2.2 12 CM CONICAL MESC THRUSTER

The 12 cm conical MESC thruster was a laboratory thruster designed for maximum flexibility in discharge chamber configuration. The thruster was designed around a 0.64 cm hollow cathode to reduce cathode overtemperature operation seen in both the hex and hemi thruster inert gas tests using a 0.32 cm diameter cathode.

The conical thruster magnet spacing tests were conducted to determine the optimum MESC magnet configuration for inert gas opertion. Leung and Hershkowitz[15] found minimum ionic losses occurred with a 1.7 cm magnet spacing under similar plasma operating condition in a slightly different discharge chamber.

2.2.1 CONICAL MESC THRUSTER CONFIGURATIONS

The 12 cm conical thruster was designed to fit an existing set of ion optics. The conical shape was selected for ease of fabricaiton, minimum wall area per discharge chamber length and rapid change in magnet-to-magnet spacing without major modifications. The magnet-to-magnet spacing of the hex and hemi MESC thruster was an integral part of the mechanical design. Any change in magnet spacing could not be accomplished without a major discharge chamber rework requiring complex machining of the discharge chamber walls. By contrast, the conical thruster magnet spacing could be changed by simply relocating the magnets and anodes in the discharge chamber.

Figure 2-5 is a photograph of the 5.7 cm long conical MESC thruster assembly, and a schematic of this assembly is shown in figure 2-6. In all, three different discharge chamber lengths were tested using the magnet spacings and anode widths shown in table 2-1.

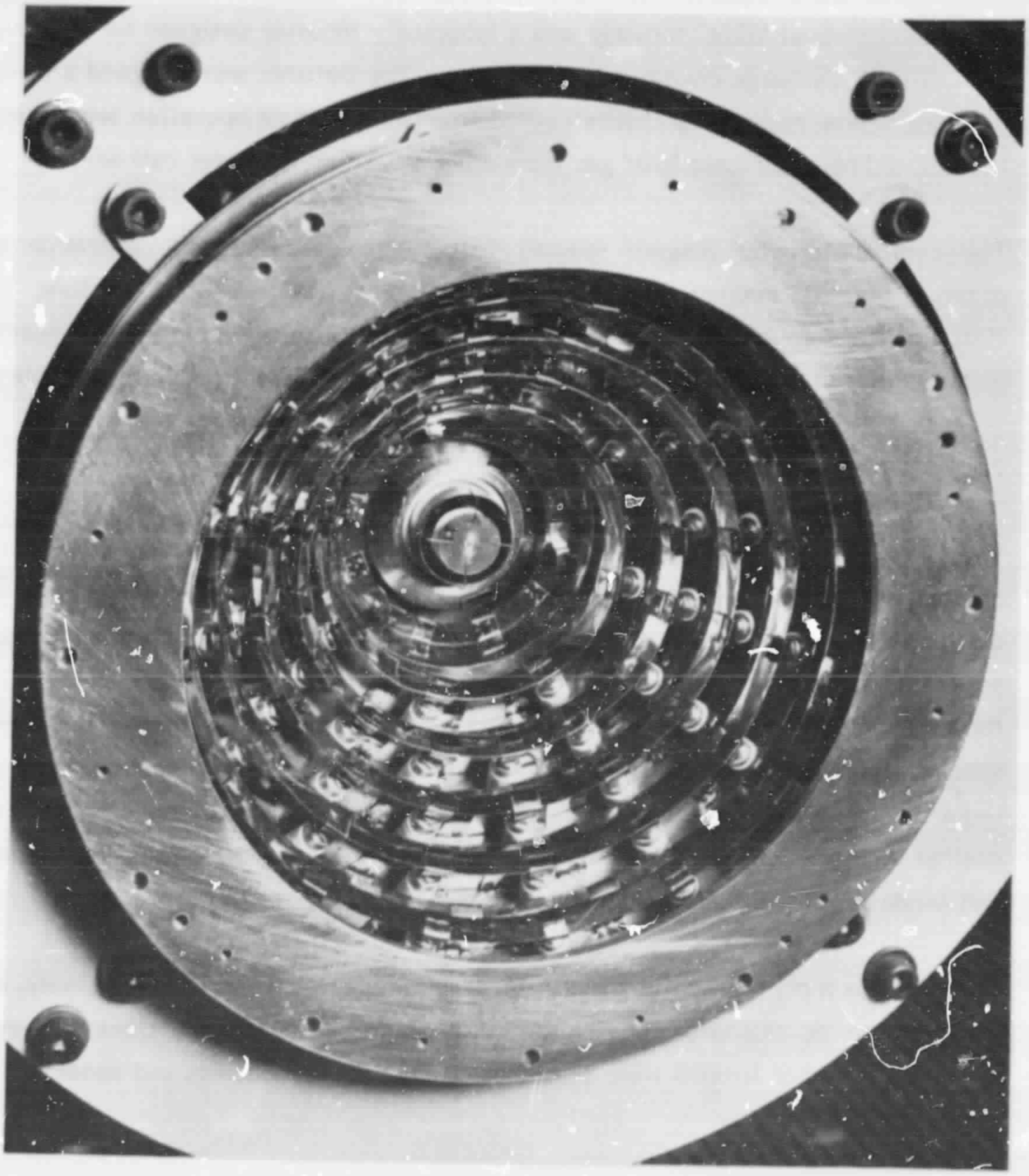

Figure 2-5. 5.7 cm Long Conical Thruster Assembly

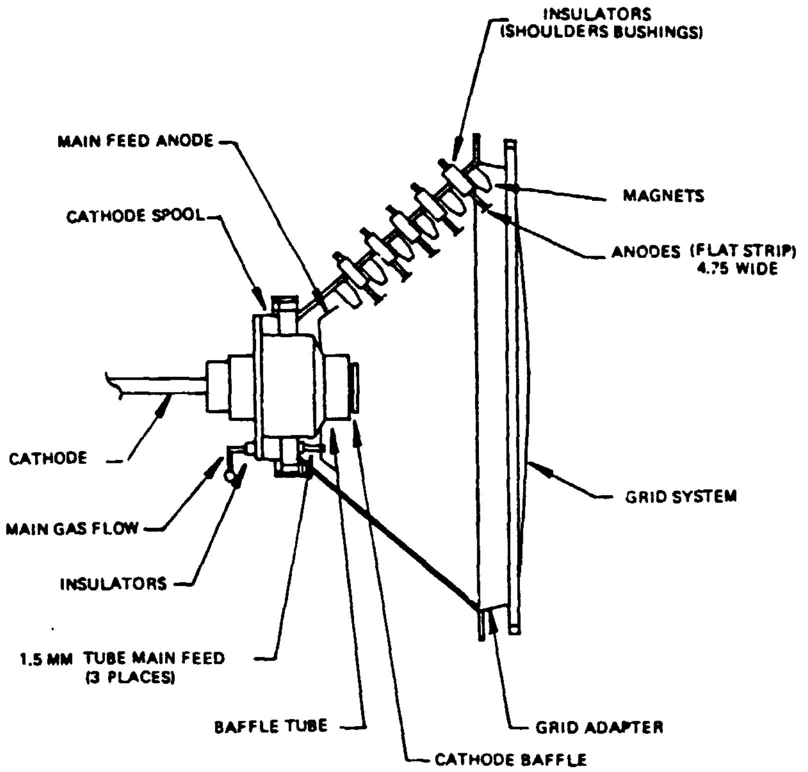

Figure 2-6. 5.7 cm Long Conical Thruster Assembly

TABLE 2-1

TEST CONFIGURATIONS

Chamber Lengths, cm	Magnet Spacing, cm	Anode Width, cm
5.7	1.3	.48
8.0	1.3-1.8	.48
9.0	2.3	.48-1.1

The 9.0 cm length discharge chamber was performance mapped with 2.3 cm magnet spacing and anode widths that ranged from 0.48 to 1.1 cm. The 9.0 cm length chamber was needed to accommodate the wider magnet spacing. The wider anode sizes were used in the 2.3 cm magnet spacing to permit better control of the anode surface magnetic flux density with the larger center-to-center magnet spacing.

A schematic of the 8.0 cm length thruster assembly is shown in figure 2-7. The 8.0 and 9.0 cm chambers used the same number of anode and magnet rows.

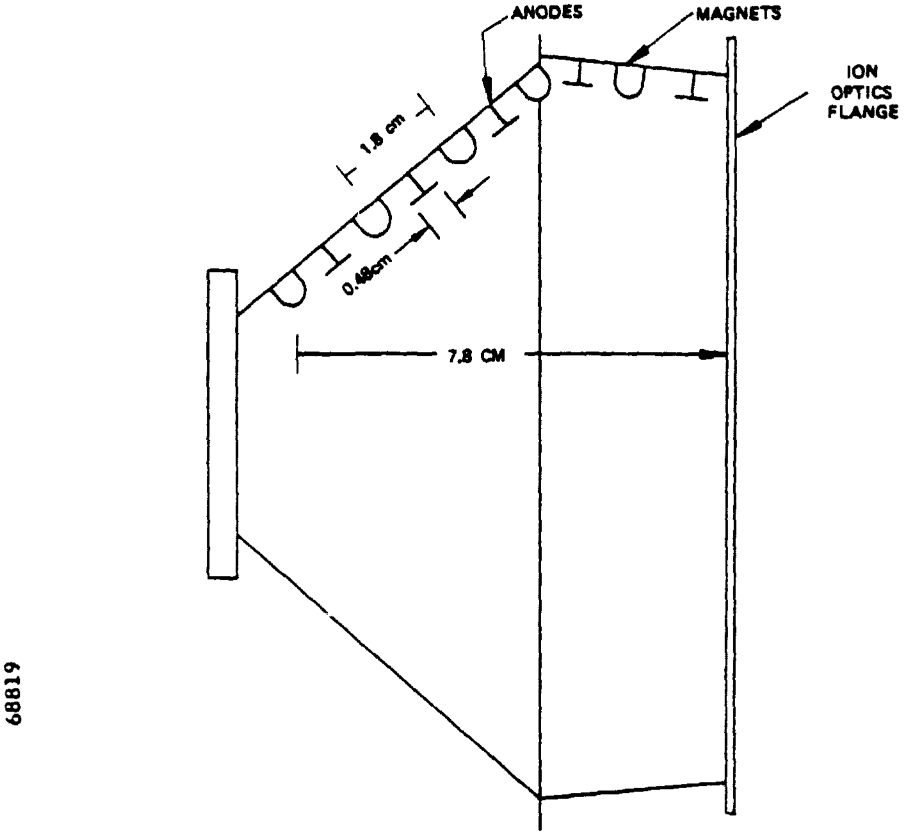

Figure 2-7. 8.0 cm Long Conical Thruster Assembly with a 1.8 cm Magnet Pitch

2.2.2 CONICAL THRUSTER 0.64 CM DIAMETER HOLLOW CATHODE ASSEMBLY

The cathode assembly used in the conical thruster was a scaled up version of the one used in the hemi and hex thruster tests[6]. A schematic of the assembly is shown in figure 2-8. The hollow cathode located on axis had a 0.5 mm diameter countersunk orifice in a 1.5 mm thick thoriated tungsten orifice plate. The orifice plate was electron beam welded to a 0.64 cm diameter molybdenum tube. The 0.45 x 0.25 x 2.5 cm long SEMICON porous tungsten emitter was held against the orifice with a 0.1 cm tantalum wire. A platinum platinum-rhodium thermocouple was spotwelded to the edge of the orifice plate to monitor the temperature. A swaged heater was used to condition the emitter and heat the cathode to operating temperature. No heater power was used during discharge operation.

Two stainless tubes were used to support and supply the electrical bias to the keeper electrode and cathode baffle disk. These tubes were concentrically located and electrically isolated from the hollow cathode and from each other by boron nitride sleeves. The keeper was a 5 mm diameter ring of 1.0 mm diameter tantalum wire suspended 2 mm from the orifice plate. Boron nitride sleeves electrically isolated the keeper support from the cathode and from the baffle support as depicted in figure 2-8. The baffle was a 1.6 cm diameter disk of 0.075 cm thick tantalum. The baffle support could be moved axially with a vacuum bulkhead control rod during thruster operation. Control rod motion located the disk between 0.84 and 1.6 cm from the cathode orifice. A third boron nitride sleeve isolated the baffle support from the cathode pole magnet so the baffle could be electrically "floated" or biased during thruster operation.

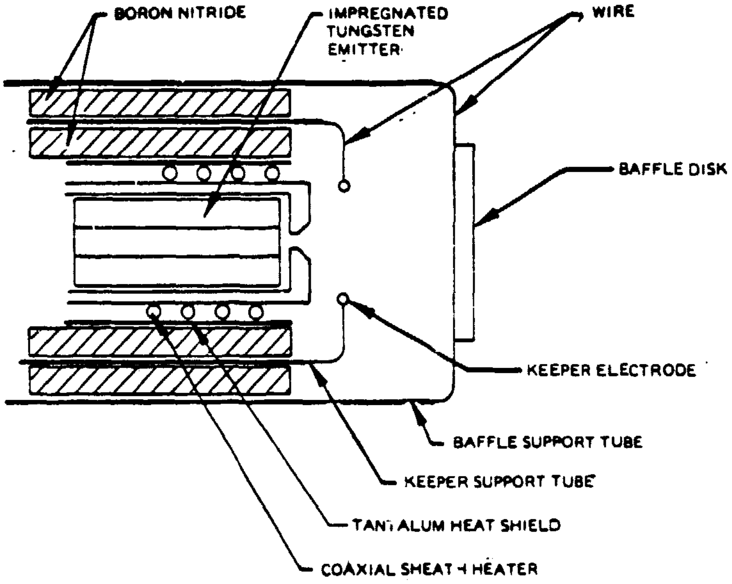

Figure 2-8. Cathode Subassembly

2.3 ION OPTICS

2.3.1 TWO GRID ION OPTICS

The hemi and conical thruster extraction grids were similar to those used during hex thruster testing^{6} except they contained 10 percent fewer holes. The corner holes found in the hexagonal array were omitted to conform more closely to the circular cross section of the hemi thruster chamber.

The two-grid small-hole-accel-grid (SHAG) design ion optics consisted of a 69 percent geometric transparent screen and 22 percent transparent accel in an uncompensated pattern. The hole diameters were 2.2 and 1.2 mm in the screen and accel, respectively. The grids were fabricated from 0.25 mm thick molybdenum which was hydroformed into a 4.0 mm deep dish for thermal stability. The grids were separated with 1.0 mm thick boron nitride washers spaced at 4.2 cm intervals around the perimeter.

2.3.2 THREE GRID ION OPTICS

The three grid ion otpics consisted of a screen grid, accel grid and a decel or ground potential grid. The decel was identical to the screen grid positioned downstream of the accel of an integrid gap ranging from 1.3 to 1.8 mm in different tests. The hole pattern was not compensated for beam divergence.

The object of the decel tests was to explore the impact of the additional grid on inert gas thruster operation and to map thruster operation at low net accelerating potentials.

2.4 GROUND SCREEN-NEUTRALIZER ASSEMBLY

The 65 cm diameter stainless steel ground screen and neutralizer assembly described in the hex thruster[6] test apparatus was used for the hemi thruster tests. The tantalum filament was slightly farther from the edge of the ion beam because the beam diameter was reduced an average of 1.0 cm due to the omitted corner holes.

2.5 TEST INSTRUMENTATION

2.5.1 POWER CONDITIONING

The power conditioning was a dc-dc inverted flight prototype breadboard designed and built on a previous program to operate at 0.5 ampere beam current and 1200 volts. The inverter drive was increased to uprate the output to 0.9 ampere at 1200 volts during the previous MESC discharge chamber inert gas program.[6] Further output increases were limited by the magnetics used in the circuit.

2.5.2 CONICAL DISCHARGE CHAMBER LANGMUIR PROBE

A 1.5 mm by 0.48 mm diameter metal sheathed Langmuir probe was used to measure discharge chamber plasma characteristics in the conical thruster. The probe was attached to a vacuum bulkhead control rod which moved the probe along the discharge chamber center line. Data were collected in the plane of each boundary anode.

An isolated dc power supply referenced to cathode potential was used to collect Langmuir probe data. An isolation transformer in the line prevented electrical breakdown between the output and chassis as the entire supply was biased to positive high voltage. Lucite control rods were used to change the supply potential and protect the operator from high voltage. Probe data were recorded on a H.V. isolated x-y plotter while manually changing dc supply potential positively and negatively with respect to the cathode reference. The probe anode numbering system used to identify probe positions is shown schematically in figure 2-9.

2.5.3 FARADAY BEAM PROBE

Three Faraday cup probes were used to measure the ion beam distribution by traversing through the beam plasma as shown in figure 2-10. A slit probe and cylindrical probe crossed the beam axis 22 cm downstream of the accel grid. A second cylindrical probe crossed 30 cm downstream of the accel grid.

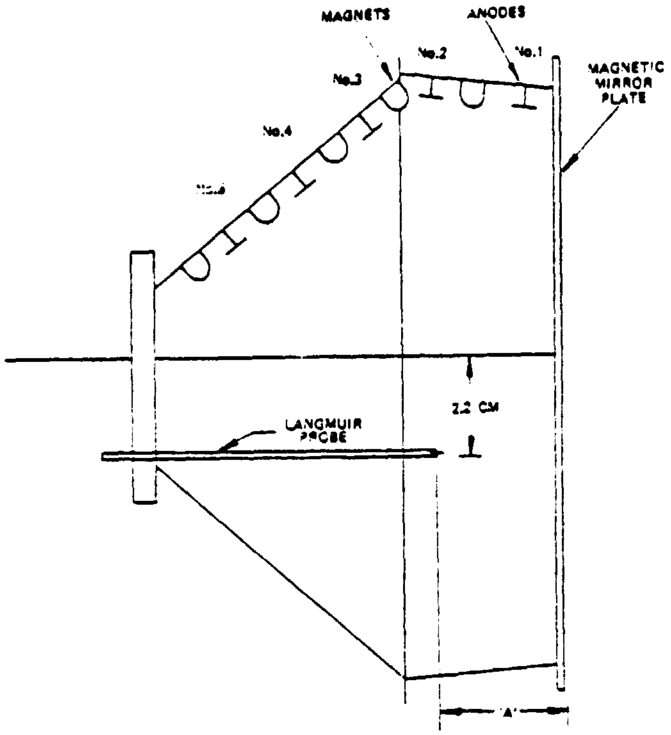

Figure 2-9. Langmuir Probe Axial Location with 1.8 cm Magnet Spacing

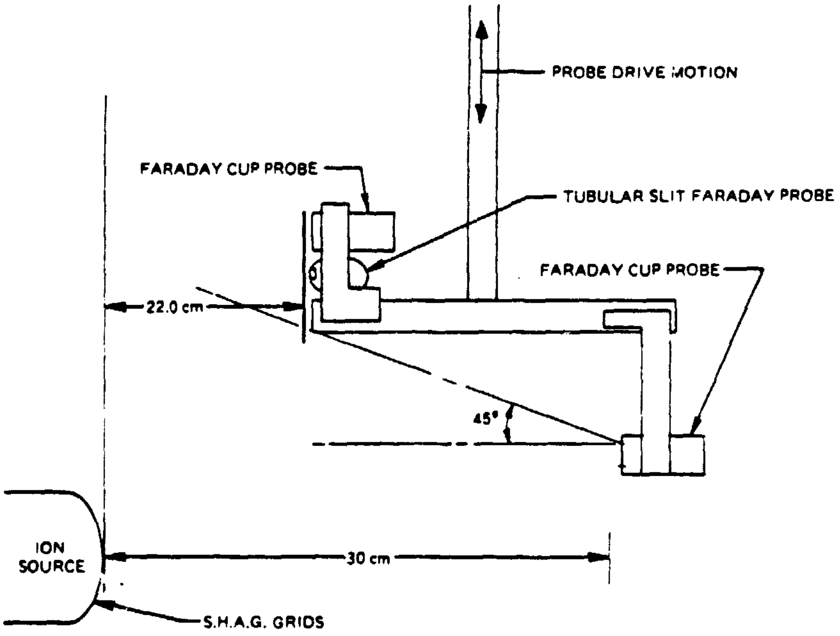

Figure 2-10. Relative Position of Faraday Probes in Ion Thruster Beam

The slit probe was used to measure beamspread and to confirm the cylindrical probe was collecting the entire beam width. The slit probe was a concentric tube assembly with a 1.27 cm diameter internal tube used as the probe collector. Electrical isolation between the tubes was accomplished by short teflon sleeves on the ends of the internal tube.

2.5.4 TIME-OF-FLIGHT COLLECTOR

Time-of-flight (TOF) data were collected to find the percentage of single and double charged ions present in the beam as a function of thruster operational parameters. Ions extracted from the discharge plasma acquire an exhaust velocity proportional to $q^{1/2}$, where q is the ionic charge. Instantaneously switching off the extraction voltage interrupts the ion current from the nominally operating discharge plasma. After interruption, a beam collector time-current profile shows two current levels as a function of time reflecting the different ionic velocities. The current level differences were used to determine relative percentage of single and double charged ion current.

The 60 cm diameter stainless steel TOF collector was located 3.4 meters downstream of the accel grid. RFI shielding was provided by a ground potential collector housing with two electrically isolated tungsten wire grids. The grids were positioned between the beam plasma and collector. The upstream and downstream grids operated at ground and negative 40 volts, respectively, to minimize collector signal noise and suppress secondary electrons. The collector operated at ground through a 1000 ohm resistor.

The double charged ion current in the exhaust beam was measured by instantaneously grounding the positive high voltage supply output and measuring the collector current as a function of time. Collector current-versus-time characteristics were measured by monitoring the potential across a resistor in the collector lead with an oscilloscope. The scope was triggered by a transient from the high voltage grounding apparatus as shown in figure 2-11 and recorded with a camera. Several traces were photographed at each stabilized gas flow.

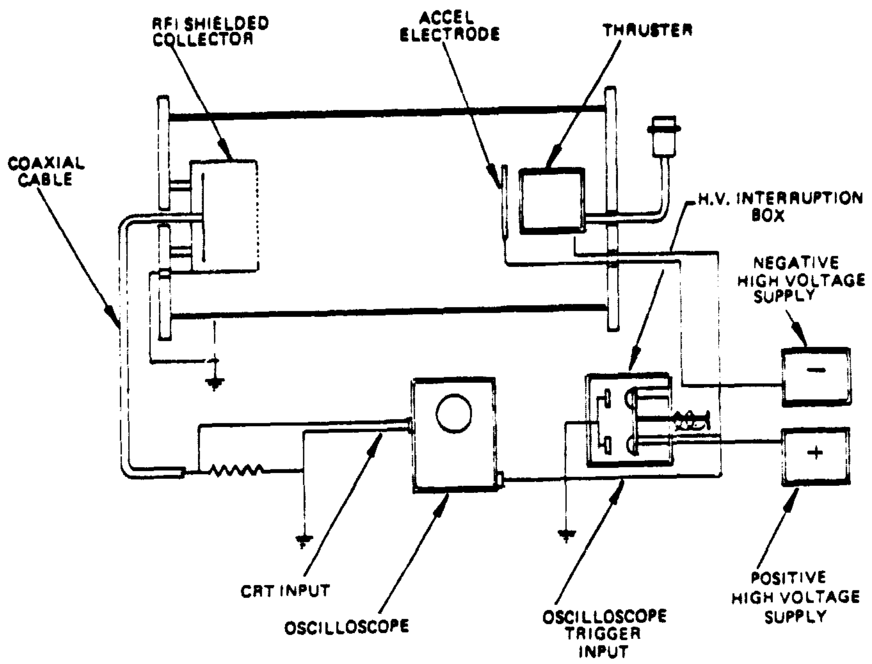

Figure 2-11. Time-of-Flight Apparatus

TOF oscilloscope traces were photographed at similar discharge current levels and different cathode-to-main flow ratios and different total mass flows and keeper potentials. The thruster operated in a constant discharge current mode during all tests. TOF data were recorded after a 0.5 or 1.0 amp change in discharge level and operational equilibrium had been established. The anode and keeper potentials were allowed to seek the levels necessary to sustain the selected discharge and keeper currents.

The scope was used in a single sweep mode with a selected sweep rate of 50 microseconds/cm. A one-to-one probe was used with a y-axis scale of 0.2 volts/cm. Times necessary to travel the 3.0 meters were computed using the kinetic energy relationship.

$$T = \frac{d}{\sqrt{\frac{2qV}{M}}}$$

Where V was the net extraction potential; M the ionic mass; q the ionic charge; and d the distance from the grids to collector.

Calculations found a 1000 volt argon beam took 43 and 30 microseconds for the respective single and double charged ions to traverse thruster-to-collector distance. Single and double charged xenon ions arrived at the collector 86.5 and 50 microseconds, respectively, after beam interruption. At 50 microseconds/cm sweep, the single and double charged argon ions current were separated by 2.6 mm and single and double charged xenon currents by 4.7 mm.

Faster sweep rates were precluded by the one-to-two cycle overcurrent response of the 20 kHz inverted high voltage supply and the stored charged in the system. Stored charge was due to system filtering that added several RC time constants, and produced a 142 microsecond current "roll off" in the current-versus-time collector profile. When the time constants added together, the collector current took as long as 320 microseconds to go to zero after the removal of high voltage. The 50 microseconds/cm sweep rate allowed the entire beam decay to be displayed while still providing adequate resolution to identify the singly charged ion current plateau.

2.5.5 GAS FLOW MEASUREMENTS AND CONTROLS

Gas flows through the thruster cathode and discharge chamber feed were controlled and measured with the same apparatus used in the previous program.[18] The flow to the cathode and main were regulated with two needle valves. Rough measurements of gas flow rates were made with rotometers in series with the valves. The mass flow transducer data were used to calculate performance. The shunt valves were used for fast feed system pump down. A schematic of the gas flow control system is shown in figure 2-12 for reference.

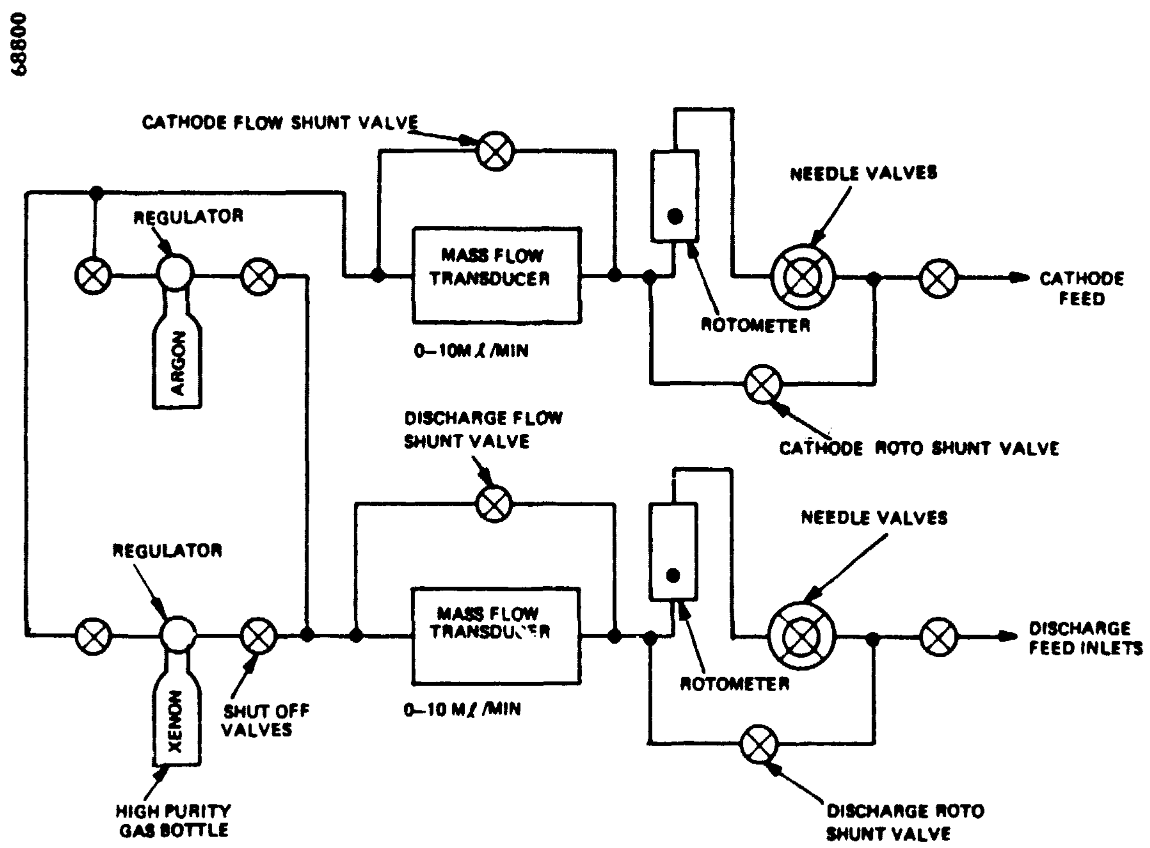

Figure 2-12. Thruster Gas Flow Control Systems

SECTION 3

TESTS RESULTS

3.1 THRUSTER TEST PHILOSOPHY

Thruster performance optimization was accomplished by varying operational test parameters in a systematic manner. Data from each test were reviewed and the extracted information was used to reconfigure the boundary anode radial position.

The boundary anode array served two purposes. For a particular discharge voltage, the anodes must be set at the position in the boundary magnetic field to minimize ionic recombination losses on the pole faces, but still collect enough electron current to sustain the discharge without producing inefficiency. For optimal performance, the arc potential must be the minimum necessary to attain high primary electron ionization probability for the molecular species being tested.

Thruster performance tests usually followed the same general procedure, with data recorded before each change of operational parameter. Once the gas flow rate was confirmed to be stable, the baffle assembly was adjusted for maximum arc current. Next, the anode current was varied in a step-wise manner from the lowest stable level to at least 5 amps. If mass utilization efficiency was 60 percent at a nominal anode potential, further data were collected. If not, the cathode discharge gas flow ratio was changed and the procedure repeated.

Test results will be presented in the following order to show the effects of various configuration changes on thruster performance when operated with argon and xenon propellent. First, an overall comparison will be made of thruster geometries tested in this and previous programs. Next, the effects of two grid and three grid ion optics will be shown. Included in that comparison will be the performance gain obtained by a uniform high strength magnetic field. The performance impact of discharge chamber length will be discussed by comparing the test results from different lengths under similar operating conditions. Finally, the effects of magnet pitch will be presented for a conical discharge chamber with some variation in chamber length.

The difficulties involved in configuration changes and constraints of time and resources precluded the execution of a complete matrix of test variables. The comparisons made in the subsequent sections are indicative however, of the relative sensitivities of these variables on thruster performance.

In the presentation of test results and discussion to follow, frequent reference will be made to thruster performance quoting mass utilization efficiency in percent and discharge losses in eV/ion. To simplify the presentation, unless otherwise stated, thruster performance will hereafter be designated simply as "efficiency of so many percent at a particular eV/ion." In all cases the mass utilization efficiency was corrected for double charged ions and back ingestion of neutral propellent from the tank environment. Discharge loss calculations included the beam current equivalent in the measured discharged current.

3.2 12 CM MESC INERT GAS PERFORMANCE

Performance mapping of the various MESC thruster configurations showed that the conical discharge chamber with a 1.8 cm pitch magnet pattern produced the most efficient discharge operation. Figure 3-1 compares the best argon performance of the 12 cm diameter MESC thruster assemblies tested. The conical thruster achieved argon efficiencies of 50 to 80 percent at 240 to 310 eV/ion. At mass utilization of 80 percent the conical thruster performance was 100 eV/ion better than sm-co magnet hemi thruster performance.

The best xenon performance was achieved in the 12 cm diameter conical MESC thruster having a 1.8 cm pitch magnet pattern. As shown in figure 3-2 it produced 60 to 97 percent utilization at 240 to 380 eV/ion. This corresponds to discharge losses ~40 to 80 eV/ion less than the hemi or hex assembly at mass efficiencies above 90 percent.

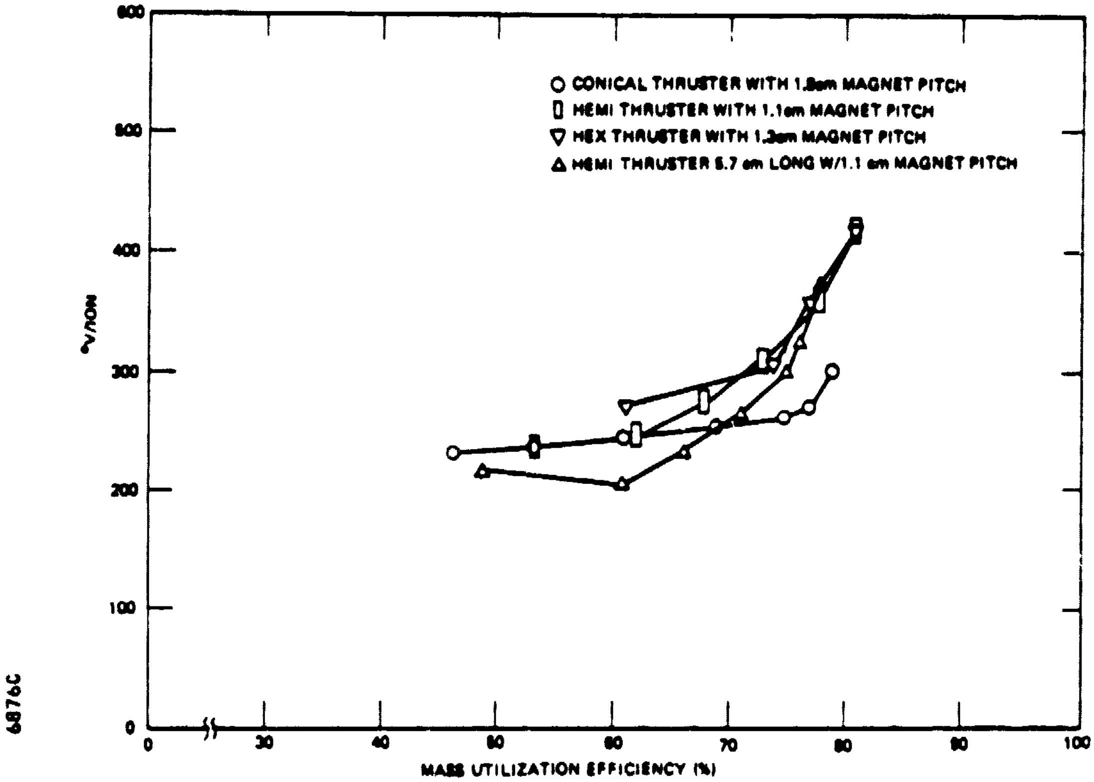

Figure 3-1. Argon Performance Comparison of 12 cm MESC Thrusters

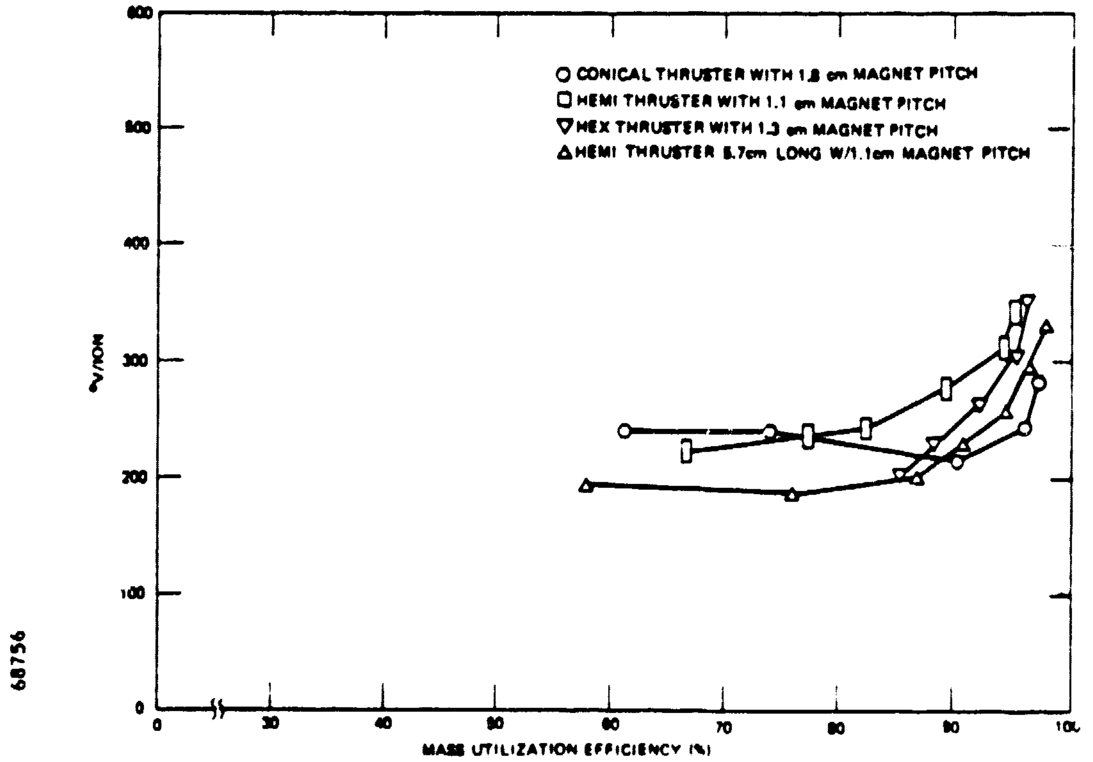

Figure 3-2. Xenon Performance Comparison of 12 cm MESC Thrusters

3.3 HEMI THRUSTER PLATINUM-COBALT MAGNET ASSEMBLY

3.3.1 TWO GRID ION OPTICS TESTS

The hemi thruster platinum-cobalt magnet assembly achieved the best performance with the boundary anode quadrants located an uneven distance from the magnets. With the anodes thus located, the magnetic field at the anode surfaces were found to have a uniform value of 7.0 millitesla.

The anode-to-magnet-pole-surface (MPS) displacement varied from 1.7 to 3.4 mm for optimum performance. Argon efficiencies of 35 to 63 percent at 300 to 410 eV/ion were achieved with the optimally placed anodes, as seen in the performance curves in figure 3-3. The knee of the argon performance curve occurred at 57 percent and 330 eV/ion. The same, optimized anode configuration was operated with xenon, and the performance results are shown in figure 3-4. Mass efficiencies were 79 to 93 percent at discharge losses of 270 to 480 eV/ion with the performance curve "knee" at 85 percent and 290 eV/ion.

3.3.2 THREE GRID ION OPTICS TESTS

The addition of the third grid to the platinum-cobalt hemi thruster magnet assembly improved argon and xenon performance. The same optimized, 7.0 millitesla anode magnetic field produced argon efficiencies of 53 to 66 percent at 300 to 380 eV/ion and shifted the performance curve knee from 57 to 65 percent. Xenon discharge losses were also reduced 20 to 60 eV/ion, compared to two grid operation. A comparison of two and three grid operation is presented for argon and xenon in figures 3-3 and 3-4.

The addition of the third grid also made it possible to operate the thruster at net accelerating potentials as low as 200 volts with net-to-total potential ratios of 0.22. Argon operation at the lowest net potentials tended to the "unstable" with spark overcurrents in the screen and accel supplies at current densities of 7.0 mA/cm^2. Lower current densities permitted smoother operation. Beamspread and beam flatness dependency on net and net-to-total extraction potentials and decel gap are discussed in the beam probe section below.

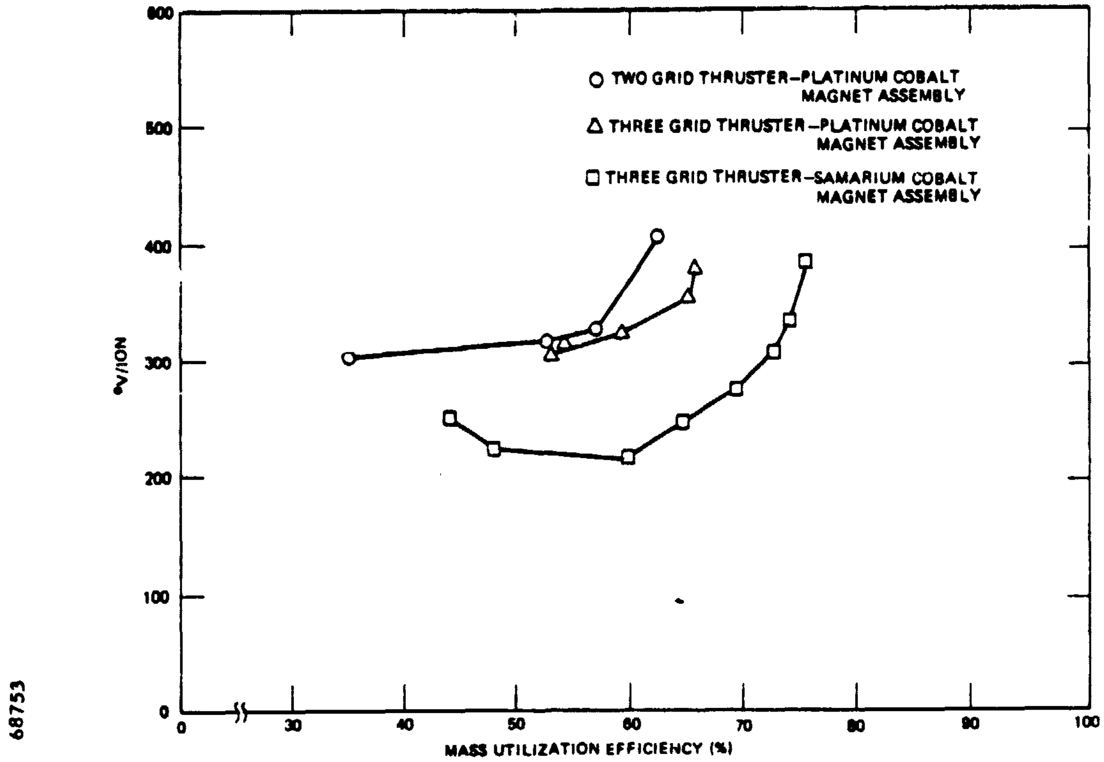

Figure 3-3. Two and Three Grid Ion Optics Argon Performance Comparison with 5.7 cm Long Thruster

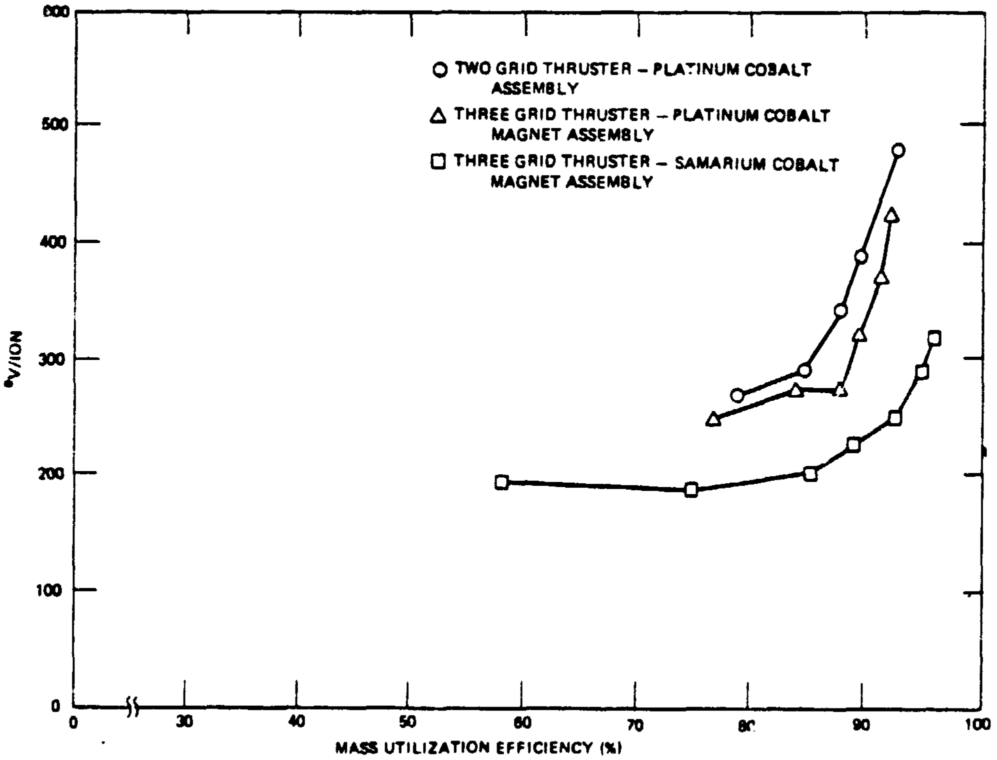

Figure 3-4. Two and Three Grid Ion Optics Xenon Performance Comparison with 5.7 cm Long Thruster

Results from argon tests showed that discharge chamber performance was related to accel-decel intergrid gap distance. With the largest gap, 2.3 mm, the performance of the three grid and two grid system were similar. Discharge losses were 18 percent higher and maximum mass utilization efficiency was 5 percent lower than the best three grid results obtained with a 1.3 mm gap. With a 1.75 mm gap, discharge losses were 5 percent higher than with the 1.3 mm gap.

The ion current incident on the decel increased proportionally to the accel-decel gap. At similar extraction potentials and beam current densities, the decel current ranged from 4.0 mA, with the 1.3 mm gap, to 22 mA with the 2.3 mm gap. Tests of the 1.75 mm gap produced decel grid currents of 12 mA. Post-test examination of the grids showed signs of direct ion impingement with severe erosion radially outward in holes along the grid perimeter. This erosion was probably caused by the absence of hole pattern compensation to correct for axial displacement of the dished grids.

Xenon operational tests with the same accel-decel gaps produced similar results. Comparing operation at 80 percent mass utilization efficiency, the discharge losses increased 8 and 17 percent for changes in grid gap from 1.3 to 1.75 mm and 1.3 to 2.3 mm, respectively. No change was observed in the maximum attainable mass utilization efficiency. All further thruster tests were conducted with three grid ion optics and 1.3 mm accel-decel gap.

3.4 HEMI THRUSTER SAMARIUM-COBALT MAGNET ASSEMBLY

3.4.1 THERMAL TEST

Because a uniform, high-strength magnetic field could not be obtained in the platinum-cobalt hemi thruster, samarium-cobalt magnets were installed as described in Apparatus and procedure. The test results to be presented here will show not only three grid optics performance but also the relative effects of optics and magnetic field design on thruster performance.

In the first test of the hemi thruster samarium-cobalt magnet assembly, discharge chamber temperatures exceeded 230°C and demagnetized the samarium-cobalt magnets. The thruster operated smoothly with apparent good performance until the discharge chamber reached 230°C. Thruster performance at temperatures >230°C rapidly deteriorated to very low mass utilization efficiency and high discharge losses with a highly nonuniform anode current distribution.

The thruster was removed from the vacuum system and carefully examined. The majority of the discharge chamber magnets were found to be demagnetized. Ten percent of the magnets had fields 1/10 of the pretest level; 50 percent had fields 1/2 or less of the original; 30 percent had fields between 1/2 and 3/4 of the original and 10 percent showed no change in field strength. Magnets in the same ring with 1/10 or less of the original field were usually flanked by magnets at the original field strength.

Thermal-vacuum tests were conducted on 10 magnet samples to determine the exact temperature of thermal demagnetization. During the tests the magnets were held at a predetermined temperature for two hours, cooled to ambient temperatures and remeasured for the residual magnetic field. Test temperatures ranged from 200° to 300° in 25°C increments. The results showed the samarium-cobalt magnets demagnetized at temperatures ranging from 250° to 300°C. Two of the sample were demagnetized after exposure to temperatures of 250°C; six magnets were demagnetized at 275°C; and two magnets demagnetized at 300°C. Thermal demagnetization occured in one irreversible drop of 50 percent or more in the residual field. Due to the uncertainty in the thermal gradient between the magnets and the discharge chamber, the maximum chamber operational temperature was limited to no more than 200°C.

Discharge chamber temperture was controlled by ambient nitrogen gas cooling and minimizing test time at maximum discharge power. Typical inlet-outlet pressure differentials of 2 to 3 atmospheres maintained discharge chamber temperature below 200°C except when discharge chamber power exceeded 200 watts. Operation above 200 watts discharge power was limited to 10 minutes or less.

3.4.2 5.7 CM HEMI THRUSTER SM-CO ASSEMBLY PERFORMANCE TESTS

The 5.7 cm long sm-co hemi thruster assembly was performance optimized by locating the anodes in increasingly stronger magnetic fields in successive tests until further increases in field strength produced argon discharge instability. Discharge instability was characterized by limited, smooth, nonoscillating operation over only a small range of total gas flow rates with higher-than-nominal anode potential. Conversely, optimum anode placement produced nominal anode operating potential over a 2:1 range of total flow rates and no discharge oscillation.

The 5.7 cm sm-co hemi thruster assembly attained optimum performance when the anode was located 6 mm from the magnets in a 9.0 millitesla magnetic field. the optimized performance shown in figures 3-3 and 3-4 corresponded to argon mass utilization efficiencies of 60 to 76 percent with total discharge losses of 215 to 385 eV/ion. The anode potential ranged from 46 to 56 volts during the argon tests.

The same anode configuration operated with xenon produced 76 to 96 percent efficiency at 185 to 320 eV/ion. Anode potentials ranged from 37 to 45 volts.

The test results shown in figures 3-3 and 3-4 indicate minor performance gains in mass utilization efficiency and discharge losses can be achieved by using 3 grid optics. A direct comparison of the optics effects was made only in the lower performance platinum-cobalt thruster. More significant gains were obtained in the uniform, high-strength samarium-cobalt magnet thruster. It is believed that a major fraction of this performance gain was due to the magnet design.

3.4.3 8.0 CM HEMI THRUSTER SM-CO ASSEMBLY PERFORMANCE TESTS

Optimized performance results of the 8 cm long thruster achieved with a 10.0 millitesla field are shown in figure 3-5. Also included in this figure are the optimized 5.7 cm long thruster data reported previously. The 8 cm thruster achieved 63 to 82 percent argon efficiency at 230 to 430 eV/ion. The knee of the performance curve occurred at about 74 percent.

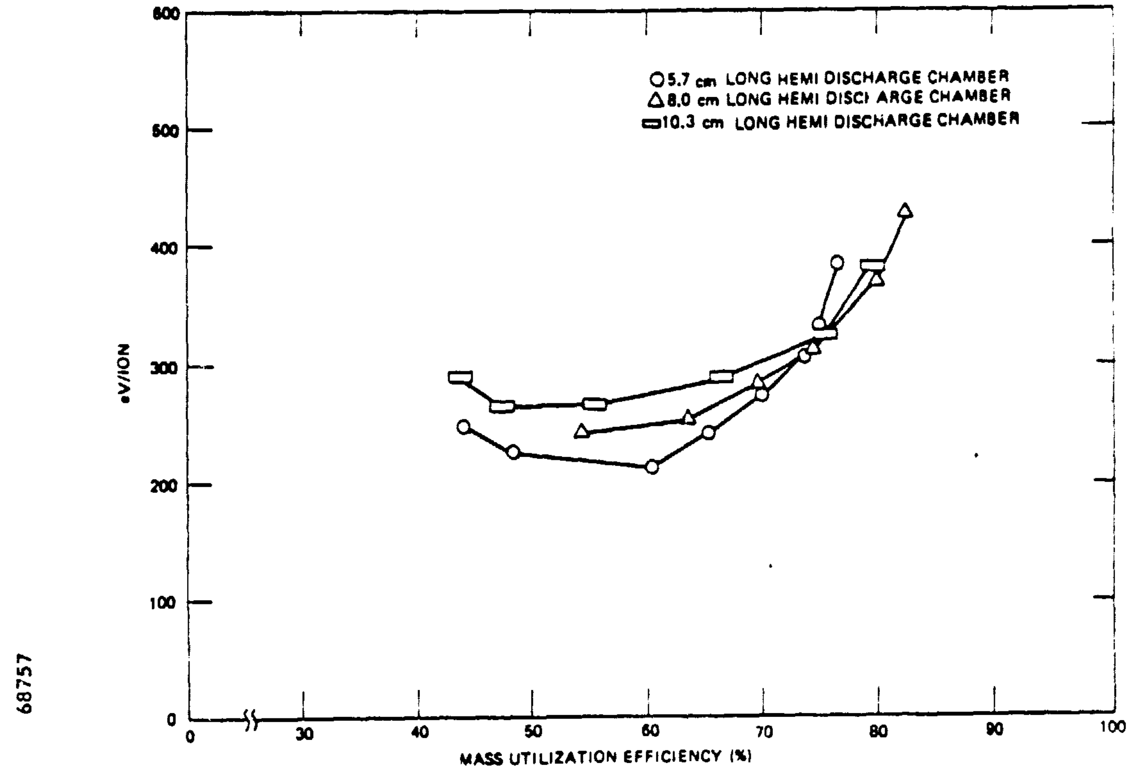

Figure 3-5. Sm-Co Hemi Thruster Discharge Chamber Length Performance Comparison in Argon

The same 10.0 millitesla anode placement achieved 77 to 95 percent xenon efficiency at discharge losses of 240 to 340 eV/ion as shown in figure 3-6. The performance curve knee occurred at about 90 percent.

Comparing the performance of the 5.7 and 8.0 cm long sm-co magnet assemblies shows that the additional length improved argon mass utilization above 74 percent but reduced xenon performance over the entire test range. The observed increases in discharge losses were probably due to higher discharge chamber recombination losses and more double charged beam ions. The latter was particularly true during xenon operation where the percentage of double charged ions increased by as much as a factor of 1.5 under similar operating conditions. This will be discussed in more detail below.

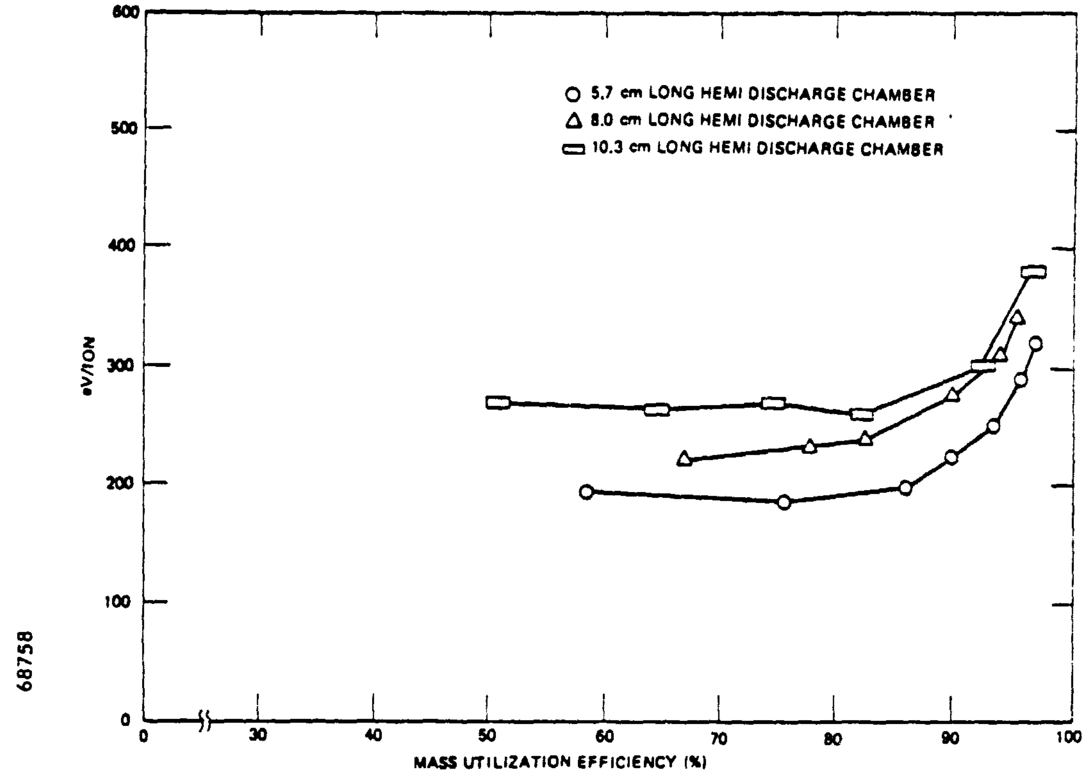

Figure 3-6. Sm-Co Hemi Thruster Discharge Chamber Length Performance Comparison in Xenon

3.4.4 10.3 CM HEMI THRUSTER SM-CO ASSEMBLY PERFORMANCE TESTS

A second 2.3 cm long spool was attached to the grid mounting flange to form a 10.3 cm long assembly. The axial magnetic field was nulled by increasing the cathode pole magnet length. Optimum performance achieved with a 12.0 millitesla anode magnetic field was 66 to 79 percent argon mass utilization at 290 to 385 eV/ion as shown in figure 3-5. Except for higher discharge losses, the performance characteristics of the 10.3 cm and 8 cm length assemblies were similar. The anode operating potential was 46 to 56 volts during these tests.

Performance of the 10.3 cm long sm-co assembly using xenon is shown in figure 3-6. Mass efficiencies ranged from 71.5 to 96 percent at discharge losses of 260 to 380 eV/ion. The anode operating potential was 37 to 45 volts and the keeper potential was 10 to 22 volts.

The reduction in xenon performance experienced in lengthening the discharge chamber was linked, in part, to an increase in the percent of double charged ions in the beam. Similar 10 cm thruster operating parameters produced a factor of 2.5 increase in double charged ions compared to the 5.7 cm length discharge chamber tests.

3.5 12 CM DIAMETER CONICAL THRUSTER PERFORMANCE TESTS

The 12 cm diameter conical thruster described in apparatus and procedure was used to investigate the effects of magnet pitch (distance between adjacent azimuthal magnets) on thruster performance. In addition, the length of the conical discharge chamber was varied over a small range to permit a comparison with the hemispherical chamber performance.

Optimized performance of all the magnet pitch - chamber length combination tested are shown in figures 3-7 and 3-8. Each configuration, however, will be presented in detail for completeness.

3.5.1 1.3 CM MAGNET PITCH IN 5.7 CM LONG CHAMBER

Performance of the 5.7 cm length assembly was optimized by the same method used in the hemi thruster tests. The anodes were positioned in the boundary magnetic field to collect the minimum electron Bohm diffusion current consistent with uniform electron current distribution to the anodes, minimum anode potential, and stable thruster operation.

The best thruster performance was seen when the anodes were located in a boundary magnetic field inversely proportional to the surface area of the individual anode strip, i.e., the furthest downstream, largest diameter anode used the lowest boundary magnetic field and smallest diameter anode had the greatest magnetic field.

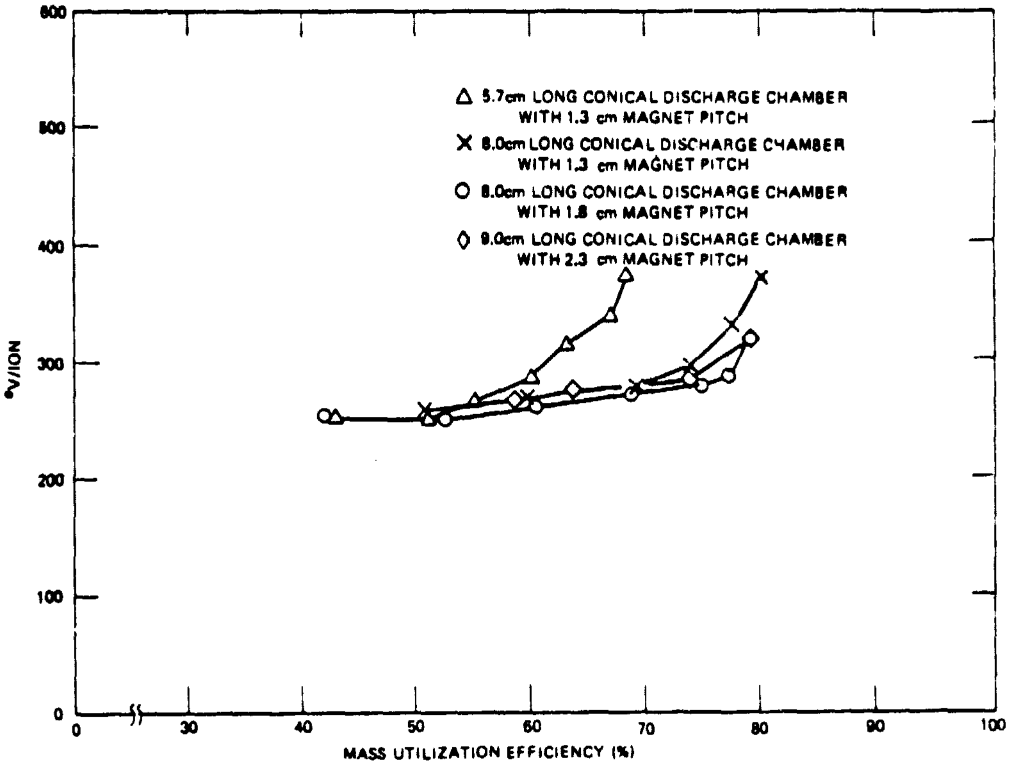

Figure 3-7. Effect of Magnet Pitch on Conical Thruster Argon Performance

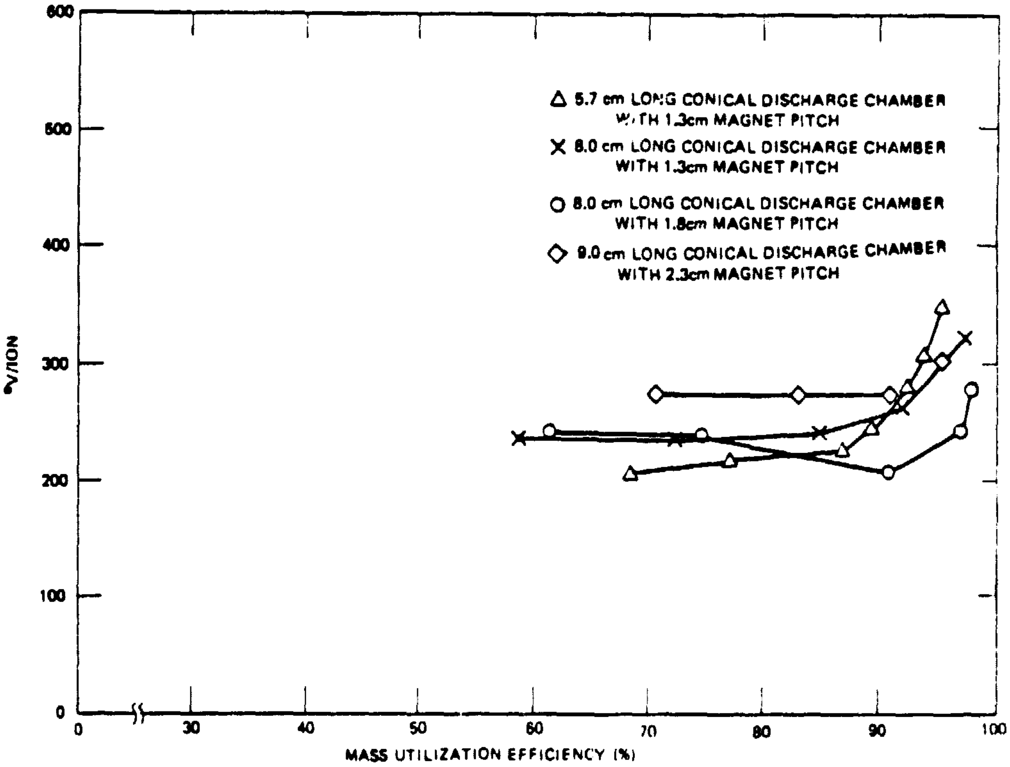

Figure 3-8. Effect of Magnet Pitch on Conical Thruster Xenon Performance

As shown in figure 3-7, optimum performance was achieved with anode fields that ranged in flux density from 8.0 to 14.0 millitesla. This anode placement produced argon efficiency of 53 to 69 percent at 260 to 365 eV/ion with anode potential of 46 to 53 volts. Xenon efficiency of 68 to 89 percent were obtained at 210 to 345 eV/ion with anode potential of 40 to 47 volts. (Figure 3-8).

Thruster performance was off-optimum when the anodes were placed in a uniform field or when the optimum anode fields were reduced 1.0 or more millitesla. Increased anode magnetic fields resulted in higher anode potential operation and discharge instability.

3.5.2 1.3 CM MAGNET PITCH IN 8.0 CM LONG CHAMBER

The best thruster performance was obtained when the anode magnetic fields were inversely proportional to the individual anode surface area. Optimum performance was seen with fields ranging from 14.0 to 19.0 millitesla. Argon performance of 62 to 81 percent efficiency and 265 to 375 eV/ion was achieved at anode potential of 49 to 55 volts. Xenon efficiency of 72 to 96 percent was obtained at 235 to 320 eV/ion with anode potential of 36 to 40 volts.

Changes in the optimum magnetic field produced the same effects seen in the 5.7 cm length tests. Reductions of 1.5 millitesla or more in the anode fields increased discharge energy consumption. Conversely, high anode fields resulted in high anode operating potentials.

3.5.3 1.8 CM MAGNET PITCH IN 8.0 CM LONG CHAMBER

Optimum anode position in this thruster assembly was calculated from the 1.3 cm magnet pitch test data. One test was needed to produce minimum eV/ion performance. The calculations were based on the total anode surface area needed to produce stable operation at minimum eV/ion with the 1.3 cm magnet pitch 8.0 cm long conical thruster assembly. The field for each anode was calculated using the simplification that the surface area seen by the diffusing electrons is proportional to the anode magnetic field.

The anode field needed in the expanded magnet pattern was calculated by assuming that a fixed total discharge current was required to achieve the maximum mass utilization efficiency. Increasing the magnet pitch reduced the number of anodes and the anode area in the discharge chamber. With the reduction in area, a proportional reduction in anode magnet field was necessary to increase the anode electron current density using the Bohm $j \propto 1/B$ diffusion current relationship.

Changing the magnet pitch from 1.3 to 1.8 cm reduced the number of anode strips in the discharge chamber from 7 to 5 and reduced the anode area exposed to the discharge. Using the Bohm relationship, the anode field was calculated to be 12.6 to 17.0 millitesla. Optimum performance was obtained with anode magnetic fields of 14.0 to 17.0 millitesla. Adjustment of the large diameter, downstream anodes was necessary to obtain optimum thruster performance. Performance of the 1.8 cm magnet pitch assembly was similar to the 1.3 cm magnet pitch except at high xenon mass efficiency.

3.5.4 2.3 CM MAGNET PITCH IN 9.0 CM LONG CHAMBER

Anode position in this thruster assembly was also calculated by using the technique described above. The magnet field for each anode was calculated and found to range from 13.0 to 16.0 millitesla for the 0.48 cm wide anodes. Optimum thruster performance was obtained with anode fields of 13.5 to 16.0 millitesla. Argon mass efficiency of 60 to 77.6 percent was produced at 273 to 360 eV/ion and xenon mass efficiencies of 74 to 94 percent were achieved at 296.

3.5.4.1 Anode Width Tests

The 2.3 cm magnet pitch configuration permitted the use of several anode widths to evaluate the effects of this variable on thruster performance. Anodes having widths of 0.48, to 0.65 and 0.86 to 1.1 cm were tested. The 0.86 to 1.1 cm anode width test used anodes of differing widths to optimize thruster performance. The calculated optimum magnetic field of each anode was used to select the anode width. The low field edge of the anodes was used to radially position the anode structure and the high field edge was trimmed to obtain an equal field.

Increases in anode width improved argon performance in the wider magnet spacing configuration. With the 0.86 and 1.1 cm anodes operating at potentials of 44 to 50 volts, argon mass utilization efficiency of 60 to 81 percent was produced at discharge losses of 260 to 310 eV/ion. Xenon operation of the same assemblies produced 75 to 95 percent at 270 to 300 eV/ion or similar to narrow anode performance. Xenon performance did not improve partly because the 9 cm length discharge chamber produced a relatively higher percentage of double charged ions than the shorter chambers.

3.5.5 THERMAL CHARACTERISTICS OF A 6.4 MM HOLLOW CATHODE

Spatial limitations restricted the hemi thruster to a 3.2 mm diameter cathode which operated beyond the recommended temperature range.[6] A 6.4 mm diameter cathode was included in the design of the conical thruster to reduce operating temperature and extend cathode emitter lifetime. Cathode temperature was monitored with two platinum-platinum rhodium thermocouples at the edge of the orifice plate and upstream of the cathode heater. Three cathode orifice diameters were evaluated in the thruster tests to identity which size produced the necessary emission currents at temperatures less than 1050°C with a minimum cathode gas flow rate. The temperature, 1050°C, was the maximum operating temperature suggested by the emitter manufacturer. Previous tests found high cathode gas flow rates were associated with high discharge losses.

Figure 3-9 shows cathode temperature plotted against cathode emission current for the three different orifice diameters. The orifice perimeter thermocouple failed open during the 0.75 mm orifice tests and the corresponding data are not included in figure 3-9. Data from three argon operational tests were used for comparison due to similarities in total flow rates and anode potential. The total mass flow averaged 0.95 amp equivalent with cathode flows of 0.46 to 0.18 amp equivalent for the 1.0 and 0.5 mm orifice tests, respectively. Anode potential was 47 to 53 volts during the tests. Keeper potential, ranged from 18 to 10 volts with the 1.8 to 4.2 amps emission current, respectively. Cathode orifice plate temperature with xenon operation was usually about 5 to 7 percent higher than with argon at similar emission currents.

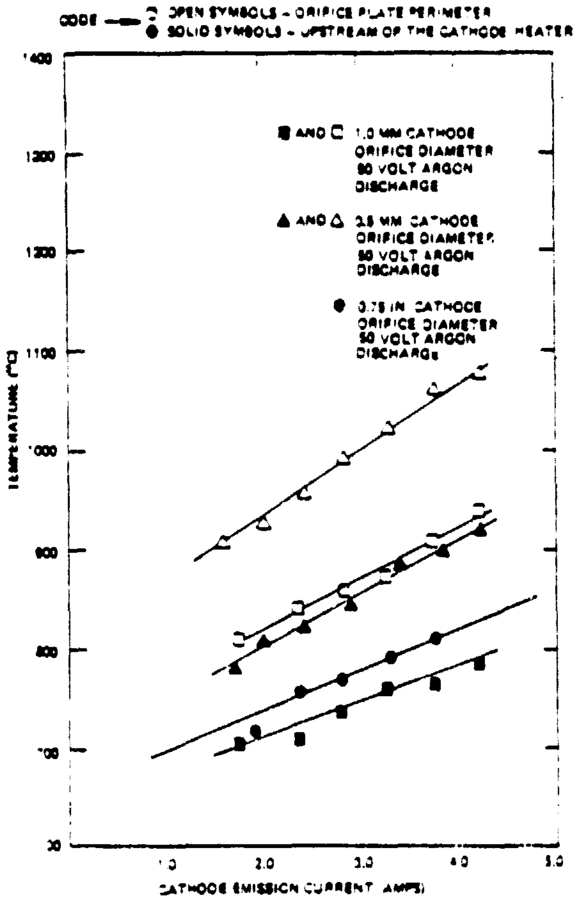

Figure 3-9. Temperature versus Emission Current for 6.4 mm Cathode Subassembly

3.6 CONICAL THRUSTER DISCHARGE PLASMA LANGMUIR PROBE DATA

Langmuir probe data were collected with the x-y plotter as described in subsection 2.5.2. Data was only collected during stable thruster operation to ensure no change in operating conditions occurred while moving the probe from one axial position to another. Typically, it took about 12 minutes to collect data from the four anode planes indicated in figure 2-9. Discharge chamber probe data were recorded for three conical assemblies having the following chamber length and magnet pitch: 8.0 cm - 1.3 cm, 8.0 cm - 1.8 cm, and 9.0 cm - 2.3 cm.

Tables 3-1 through 3-4 list the discharge plasma characteristics of the various thruster assemblies calculated from Langmuir probe data. The plasma characteristics were graphically derived from the x-y traces using the methods

TABLE 3-1

LANGMUIR PROBE DISCHARGE PLASMA DATA 1.3 CM MAGNET PITCH-8.0 CM LONG CONICAL THRUSTER ASSEMBLY

ARGON OPERATION

Data Point: 25 July 1100; I_D=4.5 amps; V_k/I_k = 22.0 volts/0.2 amp;
Σm=1.050 amps equiv

Anode Number	Anode Potential (volts)	Plasma Potential (volts)	T_{maxw} (eV)	n_{max} ($\times 10^{10}$ $\frac{\text{electron}}{\text{cm}^3}$)	T_P (eV)	n_{pri} ($\times 10^{10}$ $\frac{\text{electron}}{\text{cm}^3}$)
1	46.0	48.0	5.0	27.0	20.0	5.3
2	46.5	47.0	4.8	23.2	20.0	4.5
3	46.0	48.0	4.6	26.1	19.0	4.75
4	46.0	47.0	4.6	20.6	20.0	3.8

Data Point: 25 July 1330; I_D=2.5 amps; V_k/I_k = 18.5 volts/0.2 amps;
Σm=1.033 amps equiv

1	47.5	50.0	5.6	14.9	24.0	2.71
2	47.0	50.0	4.3	18.0	22.0	2.40
3	48.0	50.0	5.3	17.8	23.0	2.51
4	46.5	49.0	5.1	15.0	26.0	2.70

Data Point: 30 July 1645; I_D=2.0 amps; V_k/I_k = 2.6 volts/0.2 amps;
Σm=1.045 amps equiv

1	51.0	54.0	4.4	14.3	26.0	1.73
2	51.0	52.5	4.0	13.7	26.0	1.63
3	51.0	52.0	5.2	12.4	26.0	1.86
4	51.0	52.0	5.1	12.5	26.0	1.31

TABLE 3-2

LANGMUIR PROBE DISCHARGE PLASMA DATA 1.3 CM MAGNET PITCH-8.0 CM LONG CONICAL THRUSTER ASSEMBLY

XENON OPERATION

Data Point: 1 Aug 1100: I_D=2.5 amps; V_k/I_k = 21.5 volts/0.2 amps; $\Sigma \dot{m}$=0.519 amps equiv

Anode Number	Anode Potential (volts)	Plasma Potential (volts)	T_{maxw} (eV)	n_{max} ($\times 10^{10}$ $\frac{\text{electron}}{\text{cm}^3}$)	T_p (eV)	n_{pri} ($\times 10^{10}$ $\frac{\text{electron}}{\text{cm}^3}$)
1	40.5	42.5	6.8	18.3	26.0	2.31
2	40.0	41.0	6.3	15.1	26.0	1.65
3	40.5	42.0	6.6	20.2	27.0	2.60
4	40.0	42.0	6.6	17.3	25.0	1.98

Data Point: 1 Aug 1145: I_D=3.5 amps; V_k/I_k = 12.5 volts/0.2 amps; $\Sigma \dot{m}$=0.519 amps equiv

1	38.0	40.5	7.6	21.7	23.5	4.26
2	38.0	40.5	7.3	20.7	23.5	4.02
3	38.5	40.5	6.9	19.8	23.5	3.56

TABLE 3-3

LANGMUIR PROBE DISCHARGE PLASMA DATA 1.8 CM MAGNET PITCH-8.0 CM LONG CONICAL THRUSTER ASSEMBLY

ARGON OPERATION

Data Point: 2 Sept 1602: I_D=3.0 amps; V_k/I_k = 25.5 volts/0.2 amps;
$\Sigma \dot{m}$=0.974 amps equiv

Anode Number	Anode Potential (volts)	Plasma Potential (volts)	T_{maxw} (eV)	n_{maxw} $(\times 10^{10}\ \frac{electron}{cm^3})$	T_p (eV)	n_{pri} $(\times 10^{10}\ \frac{electron}{cm^3})$
1	54.0	57.5	4.8	11.2	28.5	1.16
2	54.0	58.0	5.2	15.0	28.5	0.41
3	54.5	56.0	5.6	8.78	31.0	0.84
4	54.0	57.0	4.8	1.13	32.0	0.93
5	54.0	57.5	4.8	8.62	28.0	0.81

XENON OPERATION

Data Point: 2 Sept 1130: I_D=2.8 amps; V_k/I_k = 20.0 volts/0.20 amps;
$\Sigma \dot{m}$=0.437 amp equiv

Anode Number	Anode Potential (volts)	Plasma Potential (volts)	T_{maxw} (eV)	n_{maxw} $(\times 10^{10}\ \frac{electron}{cm^3})$	T_p (eV)	n_{pri} $(\times 10^{10}\ \frac{electron}{cm^3})$
1	39.0	42.0	6.0	8.6	19.0	0.945
2	39.0	42.5	7.3	9.17	18.0	2.28
3	39.0	43.0	6.2	7.68	18.0	1.41
4	39.0	41.5	5.67	5.48	19.0	0.596
5	39.0	41.5	5.33	6.32	19.5	0.740

TABLE 3-4

LANGMUIR PROBE DISCHARGE PLASMA DATA 2.3 CM MAGNET PITCH-9.0 CM LONG CONICAL THRUSTER ASSEMBLY

ARGON OPERATION

Data Point: 8 Sept 1500: I_D=24.0 amps; V_k/I_k = 14.0 volts/0.2 amps;
Σm=1.082 amps equiv

Anode Number	Anode Potential (volts)	Plasma Potential (volts)	T_{max} (eV)	M_{max} (x10^{10} $\frac{\text{electron}}{\text{cm}^3}$)	T_p (eV)	n_p (x10^{10} $\frac{\text{electron}}{\text{cm}^3}$)
1	48.5	47.5	5.0	27.7	26.0	0.512
2	46.5	48.0	6.0	25.5	26.5	4.37
3	47.0	48.5	6.0	19.3	26.5	3.93
4	46.0	47.5	5.2	15.3	27.0	3.26
5	46.0	47.5	5.2	16.3	28.0	2.95

Data Point: 8 Sept 1335: I_D=4.0 amps V_k/I_k = 16.0 volts/0.2 amps
Σm=1.050 amps equiv

1	51.0	53.3	4.4	23.3	25.0	3.65
2	50.0	52.5	5.5	25.5	25.5	4.20
3	50.0	53.0	5.4	21.4	26.5	3.98
4	50.0	51.0	5.2	14.4	24.5	2.87
5	50.0	51.0	5.4	16.2	24.5	2.85

XENON OPERATION

Data Point: 9 Sept 1050: I_D=4.4 amps; V_k/I_k = 12.5 volts/0.2 amps;
Σm=0.667 amps equiv

1	37.5	38.0	7.0	25.1	23.0	5.0
2	38.0	39.0	6.4	31.9	23.0	5.3
3	38.0	39.0	6.2	23.9	23.0	3.48
4	37.5	35.5	5.0	20.0	23.0	2.55
5	36.5	37.5	5.8	19.8	22.0	3.11

described by Strickfaden and Geiler[17]. The tables are arranged according to thruster test assembly and further identified by test propellent. The data point cites the date and time when the Langmuir probe data was taken to facilitate correlation of thruster operating data with a given set of probe traces.

Tables 3-1 and 3-2 list the argon and xenon plasma characteristics for the 8.0 cm-1.3 cm magnet pitch respectively. Tables 3-3 and 3-4 list the plasma characteristics for the 8.0 cm long 1.8 cm magnet pitch assembly and the 9.0 cm long-2.3 cm magnet pitch assembly for the propellent indicated.

The tabulated Langmuir probe data illustrate several interesting features of the conical discharge plasma. First, it can be seen that the plasma potential was usually 1.0 to 4.0 volts greater than the applied anode potential. These results disagree with the prediction from classical physics[7] but are needed for stable operation in the Bohm diffusion realm.[12]

Second, the spatial density of Maxwellian and primary electrons were approximately proportional to the discharge current. The average of the Maxwellian and primary electron spatial density had approximately the same numerical ratio as the discharge currents in tests of the same assembly.

$$R_e = \frac{n^{(1)}_m + n^{(1)}_p}{n^{(2)}_m + n^{(2)}_p} \qquad (6)$$

$$R_D = \frac{I^{(1)}_D}{I^{(2)}_D} \qquad (7)$$

where:

$n^{(1)}_m$ or $n^{(2)}_m$ = Maxwellian electron spatial density at the initial or final test arc current

$n^{(1)}_p$ or $n^{(2)}_p$ = Primary electron spatial density at the initial or final tests arc current

$I^{(1)}_D$ or $I^{(2)}_D$ = Arc current at the initial or final test level

R_e = Electron spatial density ratio

R_D = Anode supply current ratio

For example, the 4.5 and 2.5 amp discharge current tests listed in table 3-1 had an average electron density ratio of 0.66. Discharge currents in the same two test have a ratio of 0.68. Similar ratios of 0.78 and 0.80 are produced by comparing the 2.5 and 2.0 amp discharge current tests listed in the same table. The approximation seemed to hold true for other test assemblies as well. This feature of discharge operation was used in calculating the double charge ion current produced by changes in thruster operating parameters.

Third, the potential difference between the keeper and anodes was approximately equal to the primary electron energy. This confirms the results of other workers[17] and results observed in previous tests.[18] Primary electron energy determined by the keeper to anode potential difference will be used later to calculate doubly charged ion production.

Fourth, the axial variations in electron density as determined by probe measurements were similar to the axial variations in anode current density. Figure 3-10 shows the relative electron and anode current densities derived by dividing the calculated current density by its corresponding average density. The results shown in figure 3-10 were typical of other data points. The conclusions are: first, that the Langmuir probe data yielded essentially the correct electron densities and; second, that the axial variations in plasma density along the centerline where probe measurements were made closely resembled the variations along the anode boundaries.

3.7 DOUBLE CHARGED ION MEASUREMENT

3.7.1 HEMI THRUSTER TIME-OF-FLIGHT TEST DATA

Time-of-flight (TOF) data were collected during the 5.7, 8.0, and 10.3 cm length hemi thruster sm-co assembly to determine double charged ion content. Tests were conducted at various total mass flow rates ($\dot{m}$) and cathode-to-discharge flow rate ratios ($c/\dot{m}/\dot{m}$) of 1 to 0.2 with argon and a xenon $c/\dot{m}/\dot{m}$ of 0.25 to 0 05. Typically, the anode potential increased with increases in discharge current during tests with low nominal $c/\dot{m}/\dot{m}$. Conversely, in tests with high nominal $c/\dot{m}/\dot{m}$, the anode potential decreased with discharge current. The potential difference between the keeper and anode (ΔV) increased with discharge current level.

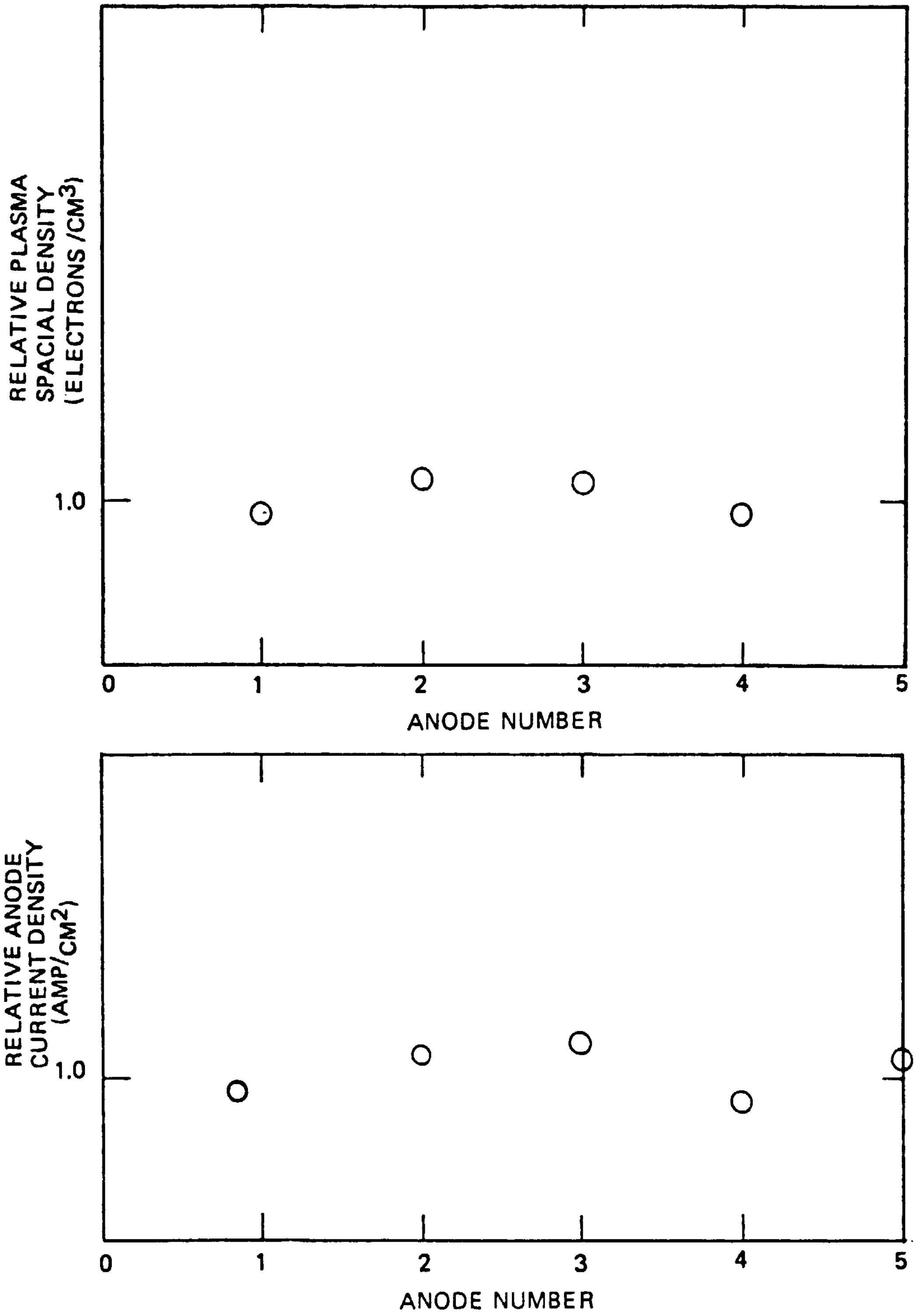

68746

Figure 3-10. Comparison of Relative Anode Current Density and Associated Plasma Spatial Density

The argon and xenon TOF data recorded during the hemi thruster performance tests are presented in tables 3-5 and 3-6. For the sake of comparison, thruster operational parameters as well as the relative percentage of double charge ion current present in the on-axis beam are shown. The tables are arranged according to thruster assembly. Further, the test data for each thruster assembly are divided into mass flow configuration groups within which the total m and the c/m/m and keeper currents are constant and only the anode current was changed.

Examination of the individual thruster assembly data revealed several interesting features of double charged ion (I^{++}) production. First, increases in discharge current tended to increase the percentage of double charge ions in the beam. Second, double charged ion current increased with the potential difference between the keeper and anodes. I^{++} did not necessarily increase with anode potential only. Third, higher mass flow rates usually produced larger percentages of I^{++}.

Comparing TOF data from the different discharge chamber assemblies indicated changing from pt-co to sm-co magnets also increased the percentage of double charged ions present in the exhaust beam. For example, changing from pt-co to sm-co magnets in a 5.7 cm long discharge chamber increased the percentage of double ion current in the beam 0.5 percent under similar operating conditions.

Increasing the discharge chamber length made a major impact on the percentage of double charge xenon ions present in the beam. Increasing the discharge chamber length from 5.7 to 8.0 cm (centerline length) increased the percentage of double charged ions by a factor of 1.5. Lengthening the discharge chamber from 5.7 to 10.3 increased the percentage of double charge ions in the beam by a factor of 2.5.

Figure 3-11 compares percentage change in the double charge argon ion current calculated using Eq. 13 of Appendix A and the percentage change observed from TOF trace data. The operational parameters needed for the calculations were taken from recorded data.

The "initial" and "final" beam and anode currents used for the calculations plotted in figure 3-5 were recorded at different anode supply currents and constant total mass flow rates. The anode supply current differences were selected at 0.5 and 1.0 amp intervals to test repeatability. A total of 40 argon operational levels were

TABLE 3-5

ARGON TIME-OF-FLIGHT HEMI THRUSTER DATA

Data Point Month/Day/Time	Anode Potential (volt)	Anode Current (amps)	Anode Keeper Potential Difference (volts)	Cathode Mass Flow (amps equiv)	Total Mass Flow (amps equiv)	I^{++}:
	8.0 CM LENGTH SAMARIUM - COBALT ASSEMBLY					
11/22/1605	46	2.5	27.0	0.640	1.046	4.0
11/22/1615	47	3.0	28.5	0.640	1.046	5.0
11/22/1620	46	3.5	28.6	0.640	1.046	6.0
11/22/1630	46	4.0	29.0	0.640	1.046	8.4
11/22/1640	46	4.5	30.0	0.640	1.046	9.0
11/22/1645	47	5.0	31.0	0.640	1.046	9.7
11/23/1002	49	2.3	27.0	0.312	1.056	4.0
11/23/1015	49	3.0	28.0	0.312	1.056	4.4
11/23/1017	49	3.5	28.0	0.312	1.056	6.6
11/23/1023	48	4.0	29.0	0.312	1.056	7.8
11/23/1032	49	4.5	30.0	0.312	1.056	9.1
11/23/1035	53	5.0	34.5	0.312	1.056	9.5
11/23/1143	51	2.0	26.0	0.355	0.638	3.3
11/23/1156	54	2.5	30.0	0.355	0.638	4.5
11/23/1204	57	3.0	33.5	0.355	0.638	5.9
11/23/1216	58	3.5	36.0	0.355	0.638	6.3
11/23/1226	58	4.0	39.5	0.355	0.638	7.6
11/23/1236	60	4.5	40.0	0.355	0.638	8.0
11/28/1350	47	2.0	29.0	0.219	0.914	4.1
11/28/1410	47	2.5	29.5	0.219	0.914	5.9
11/28/1420	47	3.0	32.0	0.219	0.914	6.9
11/28/1432	47	3.5	33.5	0.219	0.914	7.8
11/18/1438	48	4.0	35.5	0.219	0.914	8.2
11/28/1441	50	4.6	39.5	0.219	0.914	9.4
11/28/1445	52	5.0	42.0	0.219	0.914	10.7
	10.3 CM LENGTH SAMARIUM -COBALT ASSEMBLY					
12/18/1406	46	2.0	29.0	0.256	0.931	2.2
12/18/1422	47	2.5	32.0	0.256	0.931	4.0
12/18/1432	48	3.0	35.0	0.256	0.931	8.1
12/18/1435	49	3.5	36.0	0.256	0.931	9.1
12/18/1440	50	4.0	37.0	0.256	0.931	9.9
12/18/1445	50	4.5	37.0	0.256	0.931	10.6
12/18/1450	52	5.0	39.0	0.256	0.931	11.8
12/21/1132	50	2.25	26.0	0.342	0.900	3.0
12/21/1138	49	2.30	28.0	0.342	0.900	6.0
12/21/1143	44	3.25	28.0	0.342	0.900	7.6
12/21/1145	45	3.75	29.0	0.342	0.900	8.8
12/21/1148	46	4.25	33.0	0.342	0.900	9.1
12/21/1155	51	4.80	39.0	0.342	0.900	10.7
12/21/1455	49	2.25	26.0	0.242	0.609	2.6
12/21/1503	50	2.75	33.5	0.242	0.609	4.5
12/21/1510	53	3.25	38.0	0.242	0.609	7.9
12/21/1515	60	3.75	45.0	0.242	0.609	10.1

ORIGINAL PAGE IS OF POOR QUALITY

TABLE 3-6

XENON TIME-OF-FLIGHT HEMI THRUSTER DATA

Data Point Month/Day/Time	Anode Potential (volt)	Anode Current (amps)	Anode Keeper Potential Difference (volts)	Cathode Mass Flow (amps equiv)	Total Mass Flow (amps equiv)	I^{++}%
			5.7 CM LENGTH SAMARIUM - COBALT ASSEMBLY			
11/16/1015	39	2.0	26.0	0.030	0.515	2.0
11/16/1030	42	1.5	24.5	0.030	0.515	1.5
11/16/1038	39	2.5	26.5	0.030	0.515	2.6
11/16/1041	38	3.0	28.0	0.030	0.515	5.0
11/16/1045	37	3.5	28.5	0.030	0.515	5.3
11/16/1055	37	4.0	29.0	0.030	0.515	7.3
			8.0 LENGTH SAMARIUM -COBALT ASSEMBLY			
12/21/1428	39	1.9	23.0	0.020	0.632	1.3
12/21/1500	39	2.5	25.5	0.020	0.632	5.7
12/21/1505	41	3.0	28.0	0.020	0.632	6.0
12/21/1510	43	3.5	33.0	0.020	0.632	7.0
1/22/1040	33	2.45	19.5	0.059	0.546	0.0
1/22/1055	33	3.0	18.5	0.059	0.546	4.3
1/22/1100	31	3.5	20.5	0.059	0.546	5.0
1/22/1105	35	4.0	25.5	0.059	0.546	6.2
1/22/1110	34	4.5	26.0	0.059	0.546	6.6
1/22/1120	35	5.0	28.0	0.059	0.546	8.2
1/28/1125	35	2.0	24.0	0.057	0.414	2.0
1/28/1130	35	2.5	26.0	0.057	0.414	4.0
1/28/1135	37	3.0	25.0	0.057	0.414	5.0
1/28/1140	38	3.5	29.0	0.057	0.414	6.0
1/28/1143	39	4.0	33.0	0.057	0.414	9.0
1/28/1146	40	4.5	34.0	0.057	0.414	9.3
1/28/1150	43	5.0	38.0	0.057	0.414	10.0
			10.3 CM LENGTH SAMARIUM - COBALT ASSEMBLY			
2/8/1040	41	1.5	25.0	0.064	0.463	6.4
2/8/1045	38	2.0	26.0	0.064	0.463	8.0
2/8/1055	39	2.5	28.0	0.064	0.463	9.1
2/8/1115	40	3.0	31.5	0.064	0.463	12.5
2/8/1120	43	3.5	38.0	0.064	0.463	14.3
2/21/1047	34	2.0	18.0	0.055	0.452	2.3
2/21/1054	34	2.5	20.0	0.055	0.452	2.9
2/21/1056	34	3.0	21.0	0.055	0.452	4.7
2/21/1103	35	3.5	22.5	0.055	0.452	6.1
2/21/1407	39	2.1	23.0	0.051	0.615	3.0
2/21/1410	38	2.5	24.0	0.051	0.615	4.0
2/21/1415	40	3.0	27.0	0.051	0.615	6.0

compared at argon total mass flow of 0.6 to 1.1 amp equivalent. Data from all chamber lengths fell close to the full agreement line.

Calculated and observed data for 20 operating levels at xenon flows of 0.4 to 0.7 amp are shown in figure 3-12. Typically, xenon operational points under the full agreement line were taken from 8.0 and 10.3 cm long distance data and indicated more observed doubles than calculated. Those points close to or above the line were taken from 5.7 cm length test data.

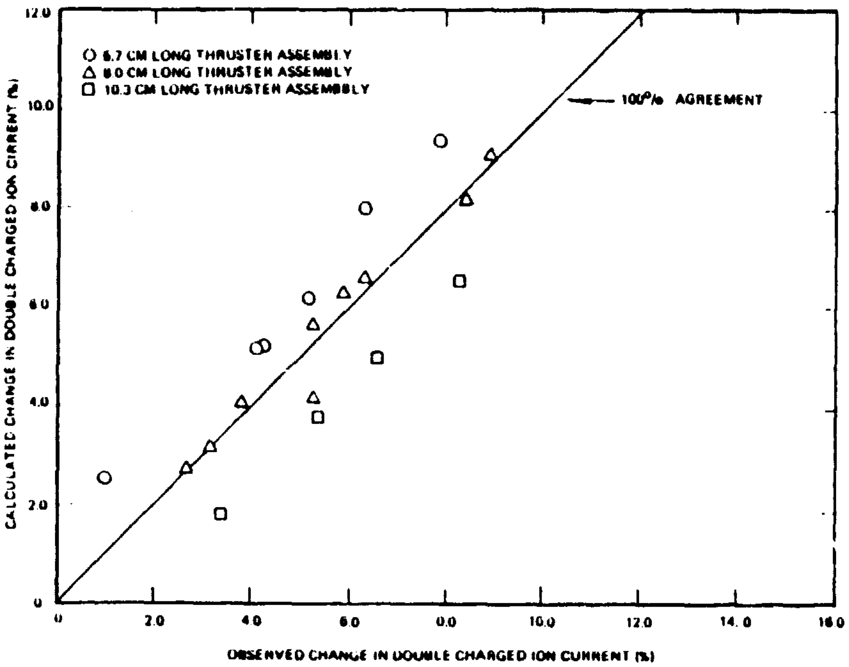

Figure 3-11. Double Charged Ion Current Comparison of Hemi Thruster Argon Operation

Equation 13 appeared to give fair approximation of the change in double ion current fraction produced by changing discharge operational parameters such as anode current, anode and keeper potential, and total mass flows. In the case of xenon, a second correction should be made for the length of the 12 cm discharge chamber. Equation 13 values will be compared with data from the operation of future MESC thruster having different volume-to-surface area ratios and discharge chamber diameters.

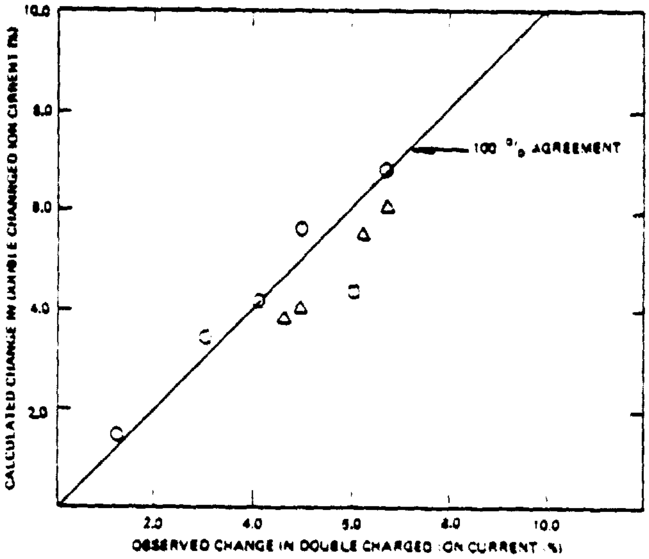

Figure 3-12. Double Charged Ion Current Comparison of Hemi Thruster Xenon Operation

3.7.2 CONICAL THRUSTER TIME-OF-FLIGHT TEST DATA

Tables 3-7 and 3-8 lists thruster operational parameters and the percentage of double charged ion current seen in the TOF data collected during those tests. The tables are arranged according to the thruster assembly being tested such as the length of the discharge chamber as well as the magnet pitch within the chamber. The individual thruster assembly data are divided into mass flow groups where the total mass ($\Sigma \dot{m}$) and the $c/\dot{m}/\dot{m}$ and the keeper current are constant and the anode current was varied similar to the hemi thruster tests.

Using Eq. 13, the relative change in double ions present in the beam was calculated from the tabulated operation parameters. A comparison of the calculated and observed double ion current is shown in figure 3-13. The calculated argon double ion current changes generally lie above the 45 degree line; i.e., fewer double charged ions were produced than the calculation indicated. A second dashed line is shown through the approximate average of the points.

TABLE 3-7

CONICAL THRUSTER ARGON TIME-OF-FLIGHT DATA

Data Point Month/Day/Time	Anode Potential (volt)	Anode Keeper Anode Current (amps)	Potential Difference (volts)	Cathode Mass Flow (amps equiv)	Total Mass Flow (amps equiv)	I^{++}:
5.7 CM LENGTH - 1.3 CM MAGNET PITCH ASSEMBLY						
4/30/1438	48	2.5	20.0	0.947	0.947	6.4
4/30/1455	47	3.5	16.0	0.947	0.947	9.6
4/30/1544	46	2.5	21.5	0.486	0.988	5.0
4/30/1553	48	3.5	25.5	0.486	0.988	6.6
4/30/1600	52	4.5	30.0	0.486	0.988	6.8
5/08/1408	51	4.0	31.0	0.305	1.027	3.7
5/08/1415	55	5.0	37.0	0.305	1.027	6.3
5/08/1435	53	3.0	31.0	0.305	1.027	4.3
8.0 CM LENGTH - 1.3 CM MAGNET PITCH ASSEMBLY						
6/27/1710	54	3.0	29.0	0.260	0.933	4.5
6/27/1730	56	4.0	35.0	0.260	0.933	7.6
6/27/1735	59	4.5	40.0	0.260	0.933	9.8
7/02/1110	53	5.0	35.5	0.400	0.982	8.6
7/02/1120	50	4.0	30.0	0.400	0.982	7.6
7/02/1130	50	3.0	26.0	0.400	0.982	6.2
7/02/1140	53	2.0	21.0	0.400	0.982	5.6
8.0 CM LENGTH - 1.8 CM MAGNET PITCH ASSEMBLY						
7/28/1630	51	1.5	24.0	0.640	1.066	0.5
7/28/1717	43	4.8	29.0	0.640	1.066	6.9
7/28/1332	51	2.0	26.5	0.558	1.005	2.1
7/28/1335	45	3.0	27.0	0.558	1.005	2.1
7/28/1400	47	4.0	30.0	0.558	1.005	6.3
7/28/1410	49	5.0	35.0	0.558	1.005	7.3
7/28/1420	49	6.0	37.5	0.558	1.005	9.5
9.0 CM LENGTH - 2.3 CM MAGNET PITCH ASSEMBLY						
9/04/1524	48	2.7	27.0	0.404	1.095	5.3
9/04/1602	50	2.0	26.0	0.404	1.095	3.7
9/04/1614	47	3.5	31.0	0.404	1.095	4.9
9/04/1630	44	5.0	38.5	0.404	1.095	7.2
9.04/1635	45	6.0	39.5	0.404	1.095	9.0
9/04/1650	53	4.7	47.0	0.250	0.964	9.0
9/04/1700	50	3.5	41.0	0.250	0.964	6.0
9/04/1710	54	2.5	42.0	0.250	0.964	4.6
9/08/1440	51	2.5	29.0	0.420	1.080	3.9
9/08/1455	49	3.5	32.5	0.420	1.080	5.2
9/08/1520	48	5.0	36.0	0.420	1.080	7.3

TABLE 3-8

CONICAL THRUSTER XENON TIME-OF-FLIGHT DATA

Data Point Month/Day/Time	Anode Potential (volt)	Anode Current (amps)	Anode Keeper Potential Difference (volts)	Cathode Mass Flow (amps equiv)	Total Mass Flow (amps equiv)	I^{++} %
5.7 CM LENGTH - 1.3 CM MAGNET PITCH ASSEMBLY						
5/02/1023	42	2.5	24.5	0.037	0.600	2.0
5/02/1105	41	3.5	27.5	0.037	0.600	3.1
5/02/1122	44	4.5	32.8	0.037	0.600	5.9
5/02/1127	47	5.0	36.5	0.037	0.600	7.2
5/02/1318	40	3.5	27.5	0.041	0.646	1.6
5/02/1328	40	4.5	32.0	0.041	0.646	4.1
5/02/1332	45	5.0	35.0	0.041	0.646	6.4
5/07/1002	41	3.0	21.0	0.047	0.646	1.1
5/07/1035	40	4.0	24.5	0.047	0.646	2.7
5/07/1042	42	5.0	29.5	0.047	0.646	4.2
8.0 CM LENGTH - 1.3 CM MAGNET PITCH ASSEMBLY						
6/28/1545	40	2.0	16.0	0.041	0.507	1.5
6/28/1600	39	3.0	20.0	0.041	0.507	3.7
6/28/1615	34	4.5	34.0	0.041	0.507	5.2
7/02/1635	36	3.0	18.0	0.027	0.671	4.5
7/02/1652	39	4.0	19.0	0.027	0.671	5.7
8.0 CM LENGTH - 1.8 CM MAGNET PITCH ASSEMBLY						
7/21/1125	39	3.0	24.0	0.054	0.656	1.7
7/21/1140	39	4.0	27.0	0.054	0.656	3.9
7/21/1145	40	4.5	30.0	0.054	0.656	5.6
7/21/1150	44	2.0	25.0	0.054	0.656	1.2
8/01/1125	41	3.0	22.5	0.049	0.536	1.9
8/01/1145	40	3.5	23.5	0.049	0.536	3.5
8/01/1215	40	4.0	27.0	0.049	0.536	5.3
8/01/1345	42	4.5	27.5	0.049	0.536	5.9
9/08/1035	39	3.0	17.2	0.034	0.667	3.3
9/08/1050	39	4.0	21.0	0.034	0.667	5.3
9/08/1110	41	5.0	24.0	0.034	0.667	7.4

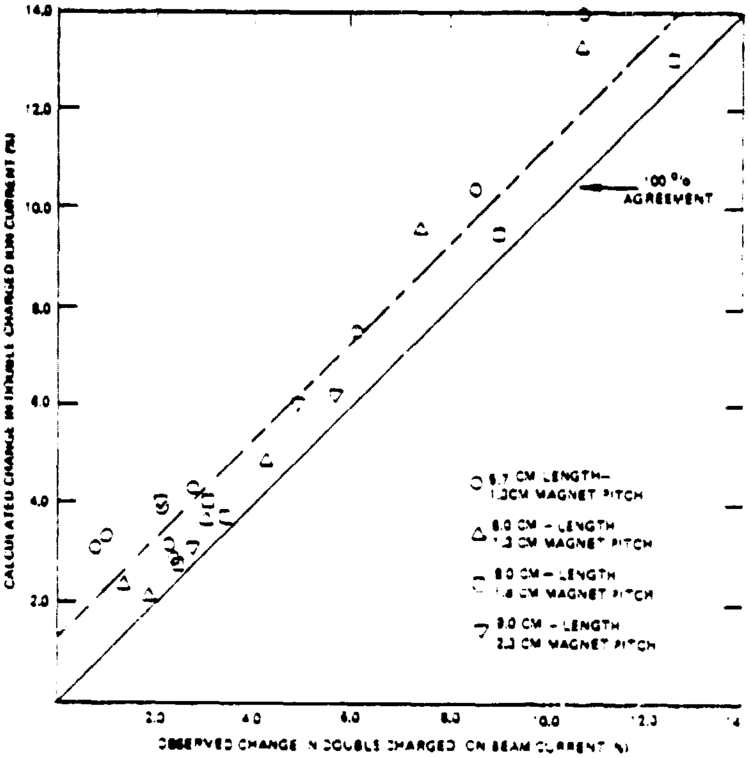

Figure 3-13. Double Charged Ion Current Comparison of Conical Thruster Argon Operation

Figure 3-14 shows the calculated change in double charged xenon ion current to the observed change in double charged ion current in the conical thruster. In this case, the points above the 100 percent agreement line are a comparison of the calculated and observed change in I^{++} for the 5.7 cm length thruster. The points on the line are a comparison of the calculated and observed values from xenon test of 8.0 meter length assembly. As in the hemi thruster tests, the test data imply longer discharge chamber residence times increase the xenon double ionization probability.

3.8 ION BEAM PROFILE MEASUREMENTS

3.8.1 HEMI THRUSTER PROBE DATA

Thruster beam profile was measured 22 and 30 cm downstream of the grid system with 1.3 cm diameter Faraday cup probes described in Apparatus and Procedure. Beamspread data were collected with two and three grid ion optics over the widest possible range of stable net extraction potentials and potential ratios. Three grid optics tests were conducted at accel-decel intergrid gaps of 1.3, 1.8 and 2.3 mm under similar thruster operating parameters.

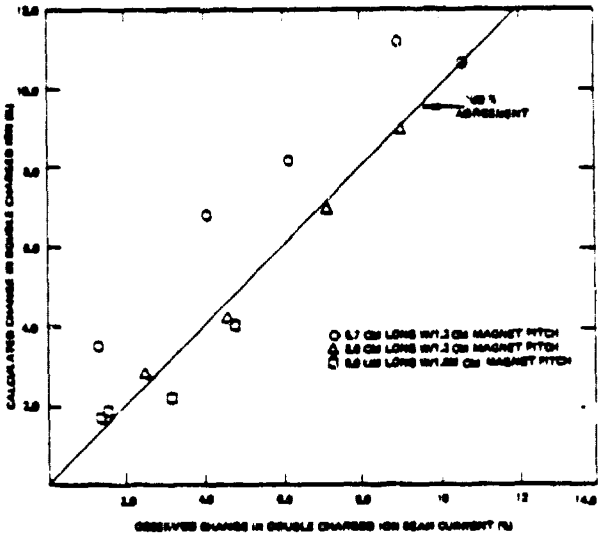

Figure 3-14. Double Charged Ion Current Comparison of Conical Thruster Xenon Operation

Table 3-9 lists the results of argon operational tests using two-grid ion optics and three grid optics with intergrid gaps of 1.3 and 1.8 mm. No differences were seen in the thruster operation with the 1.3 and 1.8 mm gaps. The two grid, test, (no decel) was run at 1100 volt total extraction potential and beam current density of 5.7 mA/cm^2. Three grid tests were conducted at 1200 volts with a beam current density of 5.5 mA/cm^2.

Table 3-10 lists the argon and xenon beam half angles obtained during tests with a 2.3 mm decel gap. The total extraction potential of 1100 volts was used in both cases. The argon tests had a beam current density of 5.4 mA/cm^2 and the xenon beam current density was 4.6 mA/cm^2.

3.8.2 CONICAL THRUSTER BEAM PROBE DATA

Beam probe data were recorded at several net-to-total extraction potentials and current densities in the conical thruster argon and xenon tests. Tables 3-9 and 3-10 list the results of these tests including net extraction potential, net-to-total potential ratios and beam half angle.

TABLE 3-9

ARGON BEAM PROFILE WITH TWO AND THREE GRIDS SYSTEMS

No. Grids	Total Voltage	Net Voltage	I_{SP}	R	Beam Half Angle	Beam Flatness
2	1100	900	2944	0.90	20	0.65
2	1100	600	2350	0.60	23	0.60
3	1200	900	2862	0.75	19	0.66
3	1200	700	2469	0.58	22	0.59
3	1200	500	2084	0.42	25	0.53
3	1200	300	1650	0.25	31	0.46
3	1200	200	1288	0.17	35	0.43

TABLE 3-10

BEAM HALF ANGLE AT TWO DECEL GAPS

Decel Gap (mm)	Extraction Potential (V)	Net Potential (V)	Argon Beam Half-Angle (degrees)	Xenon Beam Half-Angle (degrees)
2.5	1100	900	21.2	21.0
2.5	1100	800	21.9	21.9
2.5	1100	700	23.1	22.7
2.5	1100	600	23.7	23.9
2.5	1100	450	26.2	26.2
2.5	1100	300	28.0	29.0
1.75	1200	900	19.0	
1.75	1200	700	22.0	
1.75	1200	500	25.0	
1.75	1200	300	31.0	

Xenon operation produced a more uniform beam cross section than argon as can be seen by comparing the flatness coefficients in the two tables. Both xenon and argon beam spread and flatness were effected by changes in the net-to-total extraction potential and, in the case of argon, by changes in screen open area beam current density. Greater net-to-total extraction potential ratios produced less beam spread and increased the flatness coefficient. Increases in argon beam current density at the same extraction potentials slightly increased the beam spread half angle and decreased the flatness coefficient.

The probe data presented in tables 3-11 and 3-12 were collected during tests with the 5.7 cm length thruster assembly. No differences in beam characteristics were seen with longer discharge chambers or different magnet pitch patterns.

3.9 IONIC WALL LOSS TESTS

The hybrid radius hypothesis was first proposed by Leung, et al[15] while conducting tests with a slightly different "picket fence" magnet containment. Later tests at other facilities[14,16] with different experimental setups tended to confirm the hybrid radius limited ionic drift to the discharge walls. The tests described below were a small IR&D effort aimed toward defining the location and density of ion wall recombination current within an operating MESC discharge chamber. Physical changes made to the hemi discharge chamber for the wall loss tests were kept to a minimum.

The 5.7 cm long hemi thruster platinum-cobalt magnet assembly was used for the tests. Four collecting surfaces were placed in the discharge chamber midway down its length. The anodes and magnets in the hemi thruster are numbered in ascending order from the grid mounting surface. The collecting surfaces were placed under anodes 2 and 3 as well as over magnets 2 and 3. The ion collectors under the anodes were 0.56 cm diameter tantalum disks 1.0 mm from the anodes, while the magnet surface collectors were two rectangles 1.3 by 0.56 by 0.025 cm thick tantalum as shown in figure 3-15. The anodes were 3.2 mm wide tantalum ribbons. The collectors were electrically isolated from the discharge chamber walls with boron nitride shoulder bushings. Separate leads were used for the collectors. A dc power supply, floating, at high voltage was used for the collectors. A dc power supply floated at high voltage was used to apply a negative bias ranging from 5 to 50 volts to the collectors during operation.

TABLE 3-11

ARGON BEAM PROBE DATA WITH THREE GRIDS

Net Beam Potential V+ (volts)	Net-to-Total Ratio	Screen Grid Open Area Current Density J_B (mA/cm^2)	Beam Flatness	Beam Spread Half Angle (degrees)
400	0.44	5.23	0.58	25.0
500	0.56	5.29	0.63	23.0
600	0.67	5.28	0.65	22.4
900	0.70	6.34	0.69	20.2
900	0.7	6.35	0.63	21.5
900	0.7	9.64	0.61	22.8

TABLE 3-12

XENON BEAM PROBE DATA

Net Beam Potential V+ (volts)	Net-to-Total Ratio	Screen Grid Open Area Current Density J_B (mA/cm^2)	Beam Flatness	Beam Spread Half Angle (degrees)
400	0.33	5.7	0.75	27.6
600	0.5	5.85	0.84	23.4
800	0.67	5.98	0.92	20.1

Saturation ion currents were recorded at several argon mass flow rates. Ion currents to the magnet pole face and anode collectors differed by an order of magnitude during the tests.

The current density was calculated by using the following assumptions: (1) uniform current density over the entire collecting surface area (2) the disks were optically masked from the plasma by the anode structure and (3) only the hybrid radius region of the disks collected ion current. Fair experimental agreement was seen between the current density to the magnet surface and the disk using the hybrid radius assumption.

Typical argon operational tests produced 6.1 mA/cm^2 current densities at the magnet pole collector and lower densities at the disk under the anode. Disk current densities of 0.4, 0.9 and 4.0 mA/cm^2 were calculated using assumptions (1), (2), and (3) above, respectively. Although the absolute values of current density varied with total mass flow in other tests, the results were similar. Overall, fairly good experimental agreement was seen between the current density at the magnet surface and the density calculated from the hybrid radius assumption.

Hybrid radius calculations assumed the primary electron energy was equal to the potential difference between the keeper and anodes and the plasma ions energy equalled the Bohm[10] stable sheath criterion. The good experimental agreement implies a quasi-uniform ion current was collected in a loss region defined by the hybrid radius and the dimensions of the magnet.

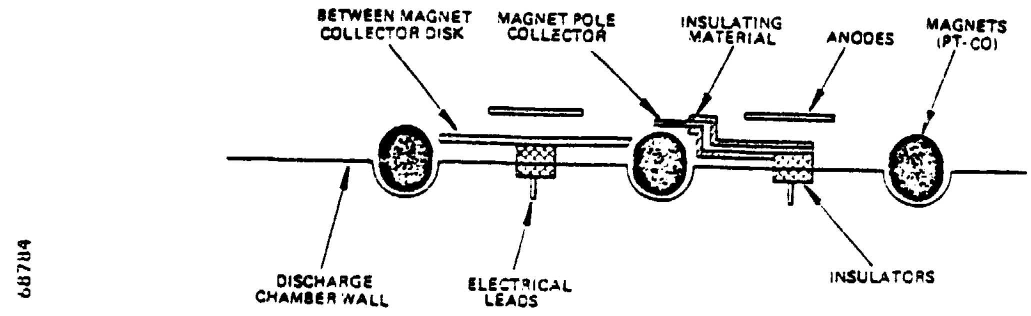

Figure 3-15. Ion Current Wall Recombination Test Apparatus

SECTION 4

DISCUSSION OF RESULTS

4.1 HEMI THRUSTER

4.1.1 PERFORMANCE IMPACT OF BOUNDARY MAGNETIC FIELD CHANGES

Changing the discharge chamber magnets in the hemi thruster from low residual field, nonuniformly magnetized platinum-cobalt magnet rings to a set of high uniform field samarium-cobalt magnets with no other thruster component change made significant differences in performance.

The best platinum-cobalt performance was limited to low argon efficiency and relatively high eV/ion. Xenon performance was not restricted to low efficiencies but discharge losses were higher than expected. The optimum anode magnetic field was 6.0 to 7.0 millitesla.

The samarium-cobalt magnet hemi thruster assembly produced the best performance with a 8.0 to 9.0 millitesla anode magnet field. Sm-co assembly tests were also conducted with 6.0 to 7.0 millitesla anode field for comparison. The results from tests with similar anode magnetic fields showed substituting the sm-co for the pt-co magnets increased the maximum argon mass utilization 11 percent, reduced the discharge energy production rate 40 eV/ion, and shifted the performance curve knee to a 10 percent greater mass efficiency. Xenon operation showed a similar encouraging trends with a 40 to 50 eV/ion reduction in discharge losses at the performance curve knee.

The two thruster assemblies differed only in the anode-to-magnet displacement and residual field of the boundary magnets. The pt-co thruster assembly required various anode radial placement to conform to the magnetic field variations. The average anode location was 0.30 cm from the magnet pole surface (mps). The average magnet residual field was 0.13 Tesla. By comparison, the anode radial location in the sm-co thruster assembly was 0.75 cm from the MPS and the average magnet residual field was 0.22 Tesla.

The ionic hybrid radius is inversely proportional to the boundary magnetic field. Hence, a greater magnetic field at the pole face results in a smaller surface recombination area. A rough calculation found the total ion recombination area was reduced ~6.4 percent by increasing the magnetic field from 0.13 to 0.22 Tesla. This calculation included the total recombination area consisting of: the screen grid webs; the grid support ring, the cathode baffle and baffle support tube; the anode area; the magnet surface area; and the surface area within the hybrid radius adjacent to the magnets.

The change in anode radial position produced a further reduction in magnet pole face recombination area. The previous interim report[18] described test results which indicated the anode-magnet geometry controlled ionic diffusion to the magnet poles. The further the anodes were from the magnets the less magnet area was available for ionic diffusion and recombination.

The magnet recombination area was calculated for the sm-co and pt-co assemblies. The calculations found the sm-co assembly total recombination area was reduced 1.7 percent compared to the pt-co assembly, due to an increase in anode-MPS displacement.

Summing up, the reduction in recombination area due to increased magnet field and anode-MPS effects was 8.1 percent. The 8.1 percent was in good agreement with the observed 8 and 10 percent shift in the performance curves.

4.1.2 8.0 CM LONG SAMARIUM-COBALT HEMI THRUSTER PERFORMANCE

The addition of one 2.3 cm length discharge spool increased the length of the samarium-cobalt hemi discharge chamber from 5.7 to 8.0 cm. Lengthening the thruster discharge impacted both argon and xenon performance. Maximum argon efficiency was increased from 75 to 81 percent and the performance curve knee moved from 69 percent at 275 eV/ion to 75 percent at 315 eV/ion. Both the changes probably reflected changes in neutral residence time and resultant increase in ionization probability.

Xenon performance of the 8.0 cm assembly showed a similar trend. The performance curve knee moved from 87 to 89.5 percent utilization and the discharge energy consumption increased from 230 to 270 eV/ion respectively. Maximum mass efficiency was uneffected by changes in discharge length but an increase was seen in the percentage of double charged beam ions. The performance curve shift as well as the increase in double ions were due to increases in discharge dimensions. Increasing the ion residence time in the highly ionized xenon plasma increased the probability of double ionization.

4.1.3 10.3 CM LONG SAMARIUM-COBALT HEMI THRUSTER PERFORMANCE

The addition of a second spool lengthened the thruster discharge chamber to 10.3 cm. The longer chamber produced some changes in argon and xenon low mass efficiency operation but made no major impact on overall thruster performance. The performance curves almost overlapped each other at argon performance between 75 to 80 percent and for xenon between 92 to 96 percent. At lower efficiencies, the 10.3 cm thruster assembly had higher discharge losses than the 8.0 cm assembly for both argon and xenon operation.

The higher losses discussed above at low mass efficiency are attributed to the following causes. First, the additional length proportionally increased the wall recombination area. The 10.3 cm assembly had a factor of 1.8 more recombination area than the 5.7 cm assembly and 1.3 times more area than the 8.0 cm length discharge chamber. Second, increases in chamber length increased the percentage of double charged beam ion, particularly during xenon operation. Comparing xenon tests with similar operational parameters but different discharge chamber lengths found the 5.7 cm, 8.0 cm and 10.3 cm assemblies produced 8, 12, and 17 percent double charged beam ions. The percentage of double charged argon ions increased from 7 to 9 percent during similar tests with the 8.0 and 10.3 cm assemblies.

4.1.4 THRUSTER PERFORMANCE WITH TWO AND THREE GRID ION OPTIC SYSTEMS

The addition of a third, or decel, grid to the ion optic system of the hemi thruster improved thruster performance. The performance curve knee and, in the case of argon, the maximum possible efficiency shifted to a larger percentage of the total mass flow. On the other hand, the thruster had the same beam spread and beam uniformity with the two and three grid systems. Performance improvement in this case was probably due to increases in neutral residence time caused by the added flow impedance of the third grid and possibly reflection of neutrals. From Dushman[21], adding the decel to the existing two grid ion optics system increased the neutral flow impedance ~25 percent. The flow impedance could probably be further increased by reducing the accel or decel grid hole diameter. Changes in the accel-decel geometry, however, may require use of a compensated grid hole pattern.

Compensated ion optics produce a more collimated beam by adjusting the radial position of individual holes in the grids. Properly focused and aligned ion beamlets should minimize grid hole diameter, maximize the neutral flow impedance, and cause no deterioration in thruster performance.

4.2 SAMARIUM-COBALT MAGNET THERMAL PROPERTIES

The hemi thruster tests and thermal vacuum tests found samarium-cobalt magnets began to demagnetize thermally at ~250°C. Demagnetization was an irreversible process and no magnet survived the 250 to 300°C test temperatures without a 90 percent loss in the original residual field. The second series of thruster tests circumvented the thermal limitations of the magnets by actively cooling the discharge chamber walls with gaseous nitrogen.

Samarium-cobalt magnets from other sources are presently under investigation in a companion IR&D program. Thermal-vacuum tests will be conducted to determine irreversible and reversible magnet field loss as a function of temperature. The preliminary results look promising as exposure to temperatures up to 350°C has had no effect on the residual magnetic field. Tests will be continued to determine the long term effect on the residual magnetic field at high temperature. If changes in the residual field can be limited to 10 percent or less, heat resistant sm-co magnets will be a promising alternative to the more massive, lower coercive force aluminum-nickel-cobalt magnets.

4.3 CONICAL THRUSTER TESTS

4.3.1 DISCHARGE CHAMBER OPERATION

The conical thruster tests showed the magnet center-to-center spacing, pitch, was important in achieving optimal discharge chamber performance. If the pitch was smaller than optimal, the greater number of magnet rows in the discharge chamber provided more magnet pole area for recombination losses. On the other hand, if the pitch was larger than optimal, the weak anode magnetic field failed to produce the electron path length needed for good ionization efficiency. Both non-optimal geometries increased the discharge eV/ion and reduced thruster performance. Optimal pitch for the conical thruster was 1.8 cm.

4.3.2 6.4 MM DIAMETER CATHODE THERMAL CHARACTERISTICS

A 6.4 mm diameter hollow cathode used in the conical thruster tests reduced the cathode emitter operating temperature. A 3.2 mm cathode had short emitter lifetime due to operation at 100 to 200°C above the 1100°C recommended by the emitter manufacturer. The 6.4 mm diameter cathode was tested with three different orifice sizes. The smallest orifice diameter, 0.5 mm, resulted in the highest orifice plate temperature of 1080°C at 4.3 amps emission current. Tests with cathode orifices of 0.75 and 1.0 mm resulted in proportionately cooler operating temperatures with the 1.0 mm diameter, having a maximum of 930°C at 4.3 amps. The larger orifice size, however, required greater cathode mass flow rates to sustain stable thruster operation at low anode potential. Typically, higher cathode mass flow operation reduced discharge chamber performance. The best thruster performance was achieved with the 0.5 mm orifice cathode.

Measurements of emitter mass loss were hampered by the hygroscopic nature of the barium-aluminate in the porous tungsten. Emitters experienced an apparent gain in mass during tests in some cases. Attempts to control the water absorption by flowing inert gas through the cathode during disassembly were not effective.

4.4 TIME-OF-FLIGHT RESULTS

Ionization theory from the literature was applied to time-of-flight (TOF) data and double charged ion beam current. Changes in macroscopic operational parameters correlated well with changes in the beam double charged ion (I^{++}) content. Knowing the I^{++} for any set of initial operational conditions, allowed the use of the ionization model to calculate changes in I^{++} for changes in thruster operating parameters with reasonable accuracy. This feature will be evaluated in future thruster performance tests. Prediction of the I^{++} from theory alone was hindered by lack of information concerning the neutral molecule and single charged ion distribution in the discharge.

4.5 CONICAL THRUSTER DISCHARGE CHAMBER LANGMUIR PROBE RESULTS

The conical thruster plasma density distribution, measured with an axial Langmuir probe, was found to agree with the anode current distribution. The probe data indicated that a greater-than-average plasma density occurred in the plane of anodes that collected greater-than-average electron current density. Relocation of the anodes produced a change in anode current distribution and a similar change in the axial plasma density. The effect of anode currents on plasma radial distribution are unknown. Plasma distribution was not affected by changes in magnet spacing. All observed results tend to confirm general plasma distribution follows the anode current distribution. This feature can be used in optimizing performance and plasma distribution in future thruster designs.

SECTION 5

SUMMARY OF RESULTS

5.1 MESC THRUSTER PERFORMANCE TESTS

The program covered by this report continued the inert gas performance tests of the 12 cm hemispherical MESC ion thruster. A new 12 cm diameter conical MESC ion thruster was designed and performance tested. Different thruster configurations were performance mapped with argon and xenon propellant to determine the best configuration. Hemi thruster tests evaluated the performance impact of two and three grid ion optics; two boundary magnet materials; and three different discharge chamber lengths. The conical thruster performance tests were conducted with three discharge chamber magnet-to-magnet spacings (pitch); three discharge chamber lengths; and different boundary anode widths.

Figure 5-1 shows the best argon performance recorded during the hemi and conical thruster tests. The best argon performance was produced with a 8.0 cm long conical discharge chamber using magnets set in rows 1.8 cm apart. The conical thruster obtained 54 to 80 percent mass utilization efficiency with discharge chamber losses of 240 to 310 eV/ion. Argon performance at less than 67 percent and minimum discharge losses was obtained with the 5.7 cm length hemi thruster fitted with samarium-cobalt magnets on 1.1 cm centers. Mass utilization efficiency was 47 to 67 percent at 230 to 260 eV/ion.

The best xenon performance observed throughout the program is shown in figure 5-2. The performance can again be divided into high and low mass utilization operation. The 8.0 cm long conical thruster with a 1.8 cm magnet spacing obtained mass efficiencies of 90 to 97 percent at 210 to 280 eV/ion. For efficiencies below 87 percent, the best xenon performance was produced with the 5.7 cm length hemi with a 1.1 cm magnet pitch.

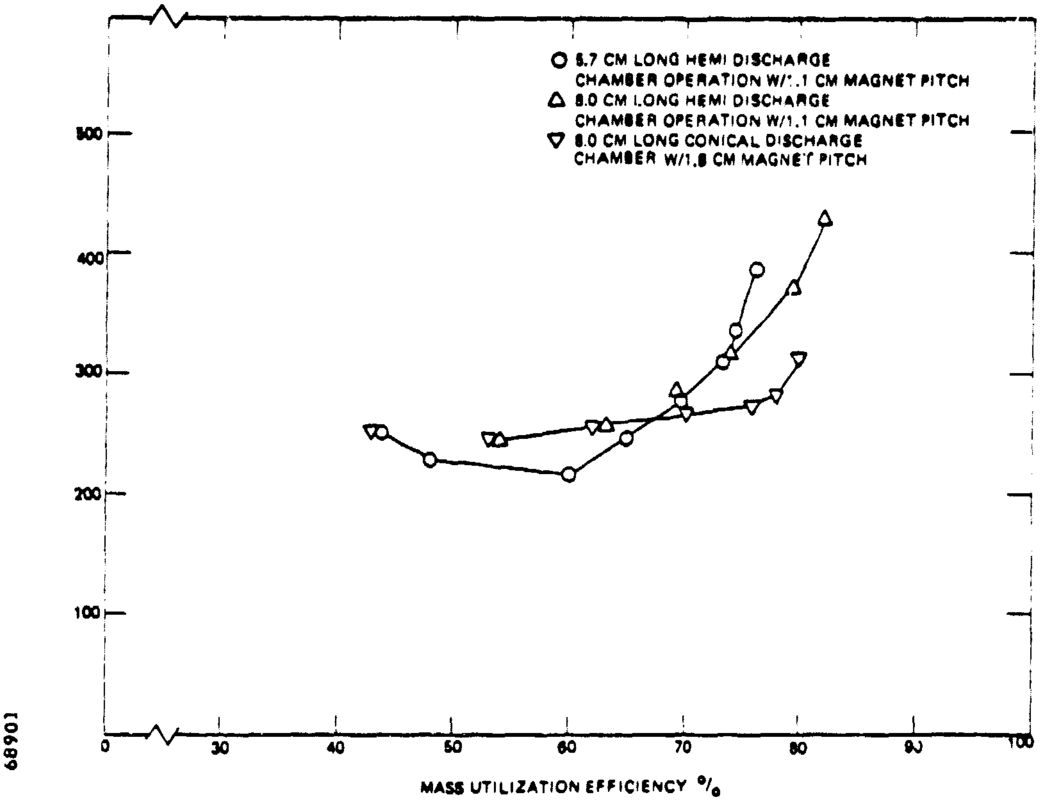

Figure 5-1. MESC Thruster Argon Operation Performance Comparison

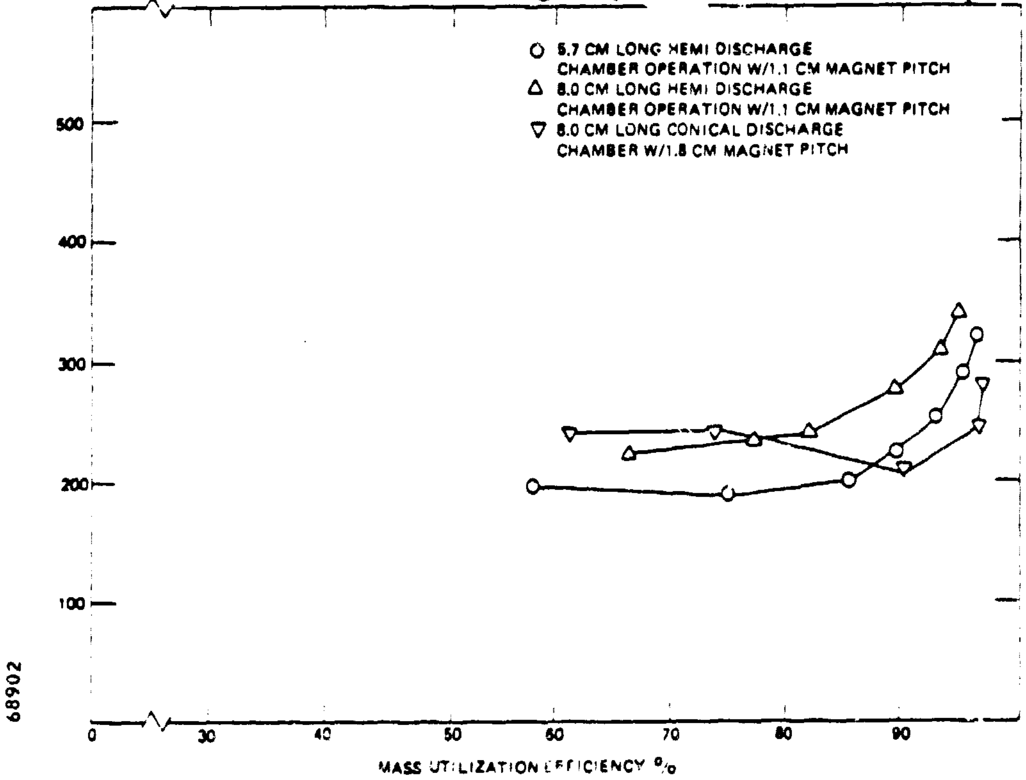

Figure 5-2. MESC Thruster Xenon Operation Performance Comparison

Hemi thruster tests were also conducted with a 10.3 cm length assembly fitted with samarium-cobalt magnets and a second 5.7 cm length hemi assembly fitted with platinum-cobalt magnets. The longer samarium-cobalt assembly had a discharge energy consumption greater than the 5.7 or 8.0 cm samarium-cobalt assembly. The 5.7 cm length pt-co magnet assembly had the greatest discharge energy consumption of any of the assemblies tested and was limited to low mass utilization argon operation. The poor performance was attributed to the nonuniform, weak, boundary magnet field produced by the pt-co magnets.

Other conical thruster tests were conducted with boundary magnet spacings of 1.3 and 2.3 cm. The 1.3 cm pitch magnets were tested in 5.7 and 8.0 cm length thruster tests assemblies, and the 2.3 cm magnet pitch was tested in a 9.0 cm length assembly. These assemblies consumed more discharge energy per mass utilization efficiency than shown in figures 5-1 and 5-2.

5.2 EXHAUST BEAM MEASUREMENTS

5.2.1 FARADAY PROBE DATA

Faraday probe measurements were used to find the beamspread and beam uniformity. No differences in beamspread or beam uniformity were seen in the data from tests with two or three grids. Beam profile characteristics were found to be a function of the accel to screen grid extraction potential ratio and the propellent species being tested. The higher ratio net-to-total applied extraction potential typically produced a smaller half angle beamspread and more uniformity than the lower ratio with either set of grids. At a net accelerating potential of 900 volts and extraction potential ratio of 0.75, argon beam half angle was 19 degrees with an average-to-peak flatness coefficient of 0.66. Similar extraction potentials with xenon produced an 18 degree beam half angle and flatness of 0.75. Compensating the radial position of the holes in the accel and decel grids for axial displacement of the grids should improve beam collimation and flatness.

5.2.2 TIME-OF-FLIGHT DATA

Time-of-flight measurements of beam ions showed the double charged ion current on axis was a function of thruster operational parameters and to a lesser extent, discharge chamber length. Test data indicated increases in the anode current and keeper-anode potential difference increased the double charged ion current. Similarly, increases in the total mass flow rate into the discharge also increased the double charged ion content. Applying ionization theory, the change in the percentage of double charged ions present in the beam could be accurately predicted from changes in the discharge operating parameters for a given discharge chamber configuration.

Changes in discharge chamber length affected the double ionization of the two propellent species differently. The percentage of argon double charged ions increased slightly in the longer discharge chamber tests. Similar operational conditions produced 9.4 and 10.8 percent doubles in argon tests of the 8.0 and 10.3 cm long sm-co magnet hemi thruster assemblies. Conical thruster argon operation produced 5.4 and 6.6 percent double charged ion current in tests with the 5.7 and 8.0 cm assembly, respectively.

Xenon operation of the three different hemi thruster assemblies produced a much larger change in the double ion beam current. Similar operational parameters produced 5.8 and 14.3 percent double charged ions in the on axis exhaust beam of the 8.0 and 10.3 cm thrusters.

In the conical thruster also, the effect of chamber length on double ion content was more pronounced with xenon than with argon. Tests with similar magnet pattern under similar operating conditions, showed the percent of xenon doubles increased from 1.1 to 4.5 percent when the discharge chamber length increased from 5.7 to 8.0 cm. Argon doubles increased from 4.3 to 6.2 percent for the same change in length.

5.3 FUTURE INERT GAS ION THRUSTER DEVELOPMENT

Tests with the present generation of MESC thrusters demonstrated several important requirements of plasma containment and plasma distribution needed for efficient thruster operation with high mass utilization and low discharge losses. The hemi thruster tests were particularly significant in demonstrating that performance improvements could be realized by increasing the boundary magnetic field flux density and uniformity. Discharge chamber designs with greater boundary magnetic fields and different magnet configurations should be pursued in future thruster development to determine what further performance gains can be obtained.

Increases in grid system gas flow impedance also improves thruster performance as demonstrated with the hemi thruster two and three grid ion optics tests. Inert gas ion optics optimization should be pursued in future development efforts to determine the best accel and decel hole diameters and hole patterns to use in the grid designs. Optimized ion optics would produce improvements in beam collimation and minimize the discharge chamber volume needed to attain high mass utilization. Minimum discharge volumes, consistent with high mass utilization operation, reduce the percentage of double charged ions in the discharge and exhaust beam as can be seen by comparing the hemi and conical thruster TOF test data.

Future thruster development effort should include an investigation into the operational characteristics of an inert gas neutralizer to ensure the orderly development of the thruster system. Several questions need to be answered which can only be gained in a neutralizer-thruster system operation. these include beam coupling potential, gas flow rates/beam current with different keeper configurations, and the thermal configuration needed for minimum input power operation. The neutralizer tests should be conducted with an operating thruster, as there is no reliable method of simulating a beam plasma.

REFERENCES

1. R. L. Poeschel et al, "High Power and 2.5 kW Advanced Technology Ion Thruster," NASA CR-135163, Hughes Research Laboratories, February 1977.
2. J. S. Sovey, "Characteristics of a 30-cm Diameter Argon Ion Source," AIAA Paper 76-1017, Electric Propulsion Conference, Key Biscayne, Florida, November 1976.
3. W. D. Ramsey, "12-cm Magneto-Electrostatic Containment Mercury Ion Thruster Development," Journal of Spacecraft and Rockets, Vol. 9, No. 5 May 1972 pp. 318-321.
4. E. L. James and W. D. Ramsey, "A Prototype North-South Station Keeping Thruster," AIAA Paper No. 74-1119, AIAA/SAE 10th Propulsion Conference, San Diego, CA, October 1974.
5. H. R. Kaufman, "Inert Gas Thrusters," NASA CR-135100 July 1975.
6. W. D. Ramsey, "Inert Gas Ion Source," NASA CR-159423 July 1978.
7. R. D. Moore, "Magneto-Electrostatically Contained Plasma Ion Thruster," AIAA Paper No. 69-260, AIAA 7th Electrical Propulsion Conference, Williamsburg, VA March 1969.
8. L. Spitzer, "Physics of Fully Ionized Gases," Interscience Publishers Inc., 2nd Revised Edition 1962.
9. W. R. Kerslake et al, "Flight and Ground Performance of the SERT II Thruster," AIAA 5th Electric Propulsion Conference, Stanford, CA August 1979.
10. A. Guthie and R. K. Wakerling, "The Characteristics of Electrical Discharges in Magnetic Fields," McGraw-Hill Book Company, Inc., 1947.
11. F. F. Chen, "Introduction to Plasma Physics," Plenium Press, 1974.
12. H. R. Kaufman, "Inert Gas Thrusters," NASA CR-159527 November 1978.
13. R. S. Robinson, "Thirty cm Ion Source," Industrial Ion Technology (H. R. Kaufman, ed) NASA CR-135149 November 1976.
14. M. G. Haines, "Plasma Containment in Cusp-Shaped Magnetic Field," Nuclear Fusion 17, 4, 1977.

15. K. N. Leung, N. Hershkowitz, K. R. MacKenize "Plasma Confinement by Localized Cusps," the Physics of Fluid, Vol. 19, No. 7, July 1976.

16. A. Kitsunezaki, M. Tanimoto, and T. Sediguchi, Phys of Fluid 17, 1974.

17. W. P. Strickfaden, and K. L. Geiler, "Probe Measurements of the Discharge in an Operating Electron-Bombardment Engine," AIAA Journal, Vol. 1, August 1963.

18. W. D. Ramsey, "Inert Gas Ion Thruster Program," NASA CR-159805, March 1980.

19. L. J. Kieffer and G. H. Dunn, "Electron Impact Ionization Cross Section Data for Atoms, Atomic Ions, and Diatomic Molecules: I Experimental Data," Reviews of Modern Physics Vol. 38, Nov. 1 Jan. 66.

20. P. J. Wilbur and H. R. Kaufman, "Double Ion Production in Argon and Xenon Ion Thrusters," J. Spacecraft and Rockets, Vol. 15, No. 4, July-August 1979.

21. S. Dushman, Scientific Foundations of Vacuum Technique, J. Wiley & Son, Second Edition 1962.

APPENDIX A

CALCULATION OF DOUBLE CHARGED ION PRODUCTION

Kieffer and Dunn[19] pointed out double ion production is linked to several discharge plasma operating processes. These include: ionization potential: neutral molecule cross section; single charged ion density; and energy levels distribution and spatial density of the ionizing electrons. Typical ion thruster discharge plasmas have two electron energy populations, a mono-energetic primary electron group at high energy and a second, larger population of electrons with Maxwellian energy distribution. The spatial density of the two groups differs by at least an order of magnitude.

The energy of the smaller, primary electron population is a function of the macroscopic discharge operating parameters related to the propellent being tested. The energy distribution of the Maxwellian population usually ranges between 3 to 6 eV, also depending on the test propellent. Electron energy level determines the ionization cross section for neutral and single charged ions. The resultant double charged ion spatial production can be expressed as follows:

$$n^{++} = n_M n_o Q_o \, dl + n_p n_o P_o \, dl + n_M n_+ Q_+ \, dl + n_p n_+ P_+ dl$$

$$n^{++} = \left[n_o (n_m Q_o + n_p P_o) + n_+ (n_M Q_+ + n_p P_+) \right] dl \qquad (8)$$

where:

n_M = Maxwellian electron spatial density

n_o = neutral molecule spatial density

n_p = primary electron spatial density

Q_o = neutral double charged ionization cross section at Maxwellian electron energy

Q_+ = single-to-double charged ionization cross section at Maxwellian electron energy

P_o = neutral double charged ionization cross section at primary electron energy level

P_+ = single-to-double charged ionization cross section at primary electron energy level

dl = ionization path lengths

n+ = single charged ion spatial density

In the above expression, the exact discharge chamber spatial density distribution of neutrals, single charged ions, and the electron populations must be known to determine the spatial density of double charged ions. It is time consuming and, in the case of neutrals, difficult to get this information in an operating thruster discharge chamber. The difficulty can be avoided by relating the doubles production to discharge macroscopic operating parameters as illustrated by work of Wilbur and Kaufman[20]. However, to use their approach, it is still necessary to know volume averaged distribution of charged particles in the discharge chamber plasma. A discharge parametric-double density relationship can also be found by noting the effect changes in discharge operation have on double charged ion beam current. Although the absolute density of double charged ions cannot be found by this method, it should indicate the double charged density change that will be realized through changes in discharge operating parameters.

Assuming:

a. Increases in discharge current increase the Maxwellian and primary density but maintained the same ratio between the two populations (see equation 5 and 7 test results section).

b. An increase in ion density equals the reduction in neutral density at fixed mass flow rates.

c. Primary electron temperature equals the potential difference between the keeper and anodes[13].

d. Increases in single and double charged ion density are proportional to increases in single and double charged beam currents.

Using the above assumption Eq. 8 becomes:

$$\frac{\Delta n^{++}}{dl} = \Delta n_o(\Delta n_M Q_o + \Delta n_p P_o) + \Delta n_+(\Delta n_M Q_+ + \Delta n_p P_+) \tag{9}$$

Comparing TOF data from operation at a constant mass flow rate the following approximations can be made:

$$\text{Let } \Delta n_o \quad \alpha \left(1 - \frac{J_b'' - J_b'}{\Sigma \dot{m}}\right) \tag{10}$$

where

J_b'' = final beam current
J_b' = initial beam current

That is, the change in neutral density is proportional to the ratio of beam current change to total mass flow rate. Using assumption a:

$$\Delta n_m \quad \alpha \left[1 + \frac{(I_d'' - I_d') - (J_b'' - J_b')}{I_d' - J_b'}\right] \frac{n_m}{n_m + n_p} \tag{11}$$

and

$$\Delta n_p \quad \alpha \left[1 + \frac{(I_d'' - I_d') - (J_b'' - J_b')}{I_d' - J_b'}\right] \frac{n_p}{n_m + n_p} \tag{12}$$

Simplify letting

$$X = \left[1 + \frac{(I_d'' - I_d') - (J_b'' - J_b')}{I_d' - J_b'}\right]$$

and

$$F_M = \frac{n_m}{n_M + n_p}$$

$$F_p = \frac{n_p}{n_M + n_p}$$

Substituting

$$\Delta n_M \propto X F_M$$

$$\Delta n_p \propto X F_p$$

where

I''_d = final anode supply current
I'_d = initial anode supply current

That is, the change in Maxwellian or primary electron plasma density is proportional to the percentage change in cathode emission. This approximation only applies to data from points fairly close together on the performance curve or from portions above and below the performance curve knee. The change in ion spacial density can be approximated by:

$$\Delta n+ \quad \propto \quad \left(1 + \frac{J''_b - J'_b}{J'_b}\right) n+$$

or the change in single charged ion plasma density is proportional to the percentage change in beam current. Substituting into (9):

$$\frac{\Delta n^{++}}{di} \propto \left[\left(1 - \frac{J''_b - J'_b}{\Sigma \dot{m}}\right) \left(F_M Q_o + F_p P_o\right) + \left(1 + \frac{J''_b - J'_b}{J'_b}\right) \left(F_M Q_+ + F_p P_+\right)\right] X$$

Hence, the change in double charged ion beam current can be approximated from operational parameters and specie ionization crossection if small changes are made in the operating parameters. Time-of-flight data used for comparison were taken from thruster data with anode supply currents that differed by .5 amps or less.